

Beamforming Design for Target Sensing and Proactive Eavesdropping

Qian Dan, Hongjiang Lei, Ki-Hong Park, Gaofeng Pan, and Mohamed-Slim Alouini

Abstract—This work studies the beamforming design in the joint proactive eavesdropping (PE) and target sensing (TS) systems. The base station (BS) wiretaps the information transmitted by the illegal transmitter and sends the waveform for TS. The shared waveform also serves as artificial noise to interfere with the illegal receiver, thereby achieving successful PE. We firstly optimize the transmitting beampattern of the BS only to maximize the eavesdropping rate or only to minimize the Cramér-Rao bound, respectively. Then, the joint design of PE and TS is investigated by formulating the PE-centric, the TS-centric, and the normalized weighted optimization problems. The formulated problems are solved by the semi-definite relaxation technique and the sequential rank-one constraint relaxation method to address the complexity of the original problem. Furthermore, the scenario in which the quality of the eavesdropping channel is stronger than that of the illegal channel is considered. Numerical simulation demonstrates that the proposed algorithm can effectively realize PE and TS simultaneously.

Index Terms—Joint proactive eavesdropping and target sensing system, beamforming design, eavesdropping rate, Cramér-Rao bound.

I. INTRODUCTION

A. Background and Related Works

Integrated sensing and communication (ISAC) technology can share spectrum, hardware platforms, and even baseband waveforms and signal processing between communication and sensing to improve the spectral efficiency, energy efficiency (EE), and hardware efficiency of the system for integration gain. Further, the mutual assistance and mutual gain of the two functions can also be used to improve each other's performance and obtain coordination gain [1]-[5].

Manuscript received.

This work was supported by the National Natural Science Foundation of China under Grant 62171031 and 61971080, National Key Research and Development Program under Grant2024YFC3306800, and Chongqing Natural Science Foundation Innovation and Development Joint Fund under Grant 2025NSCQ-LZX0066. (Corresponding author: *Hongjiang Lei*).

Qian Dan is with the School of Communications and Information Engineering, Chongqing University of Posts and Telecommunications, Chongqing 400065, China, and also with the School of Computer Science, Jiangxi University of Chinese Medicine, Nanchang 330004, China (e-mail: danqian@jxutcm.edu.cn).

Hongjiang Lei is with the School of Communications and Information Engineering, Chongqing University of Posts and Telecommunications, Chongqing 400065, China, also with the Chongqing Key Laboratory of Mobile Communications Technology, Chongqing 400065, China (e-mail: leihj@cqupt.edu.cn).

Gaofeng Pan is with the School of Cyberspace Science and Technology, Beijing Institute of Technology, Beijing 100081, China (e-mail: gfp-an@bit.edu.cn).

Ki-Hong Park and Mohamed-Slim Alouini are with CEMSE Division, King Abdullah University of Science and Technology (KAUST), Thuwal 23955-6900, Saudi Arabia (e-mail: kihong.park@kaust.edu.sa, slim.alouini@kaust.edu.sa).

Recently, the performance for various ISAC systems was investigated to achieve concurrent sensing and communication, which were classified into the radar-centric systems [6]-[10], the communication-centric systems [11]-[13], and the joint-design systems [14]-[15]. The authors in [6] investigated beamforming designs for the ISAC systems with multiple communication users for scenarios with point or extended targets. In particular, the Cramér-Rao bound (CRB) of the azimuth angle or the response matrix of the target was minimized by designing the dual-functional beamforming matrix. In [7], a new angular waveform similarity metric was proposed and combined with the integrated main-lobe-to-sidelobe ratio of the transmit beampattern to evaluate the waveform ambiguity properties. The complementary waveform and linear precoder matrix were jointly designed to minimize the weighted sum of the integrated main-lobe-to-sidelobe ratio while considering a predefined signal-to-interference-plus-noise ratio (SINR), power, and peak-to-average-power ratio constraints. In [8], the authors investigated the performance of the ISAC systems with multiple targets and communication users. Both the scenarios without and with prior target knowledge at the base station (BS) were considered, and the multi-target response matrix and the reflection coefficients/angles were estimated, respectively. The CRB of multi-target estimation was minimized while satisfying the constraints of a minimum multicast communication rate and a maximum transmit power. The authors in [9] proposed a new robust beamforming scheme for ISAC systems with different point targets. The maximum CRB of the estimated direction of arrival was minimized by designing the beamforming matrix while ensuring the quality-of-service (QoS) for all the communication users. The authors in [10] proposed an integrated sensing, communication, and computation over-the-air framework to enable simultaneous communication, target sensing (TS), and over-the-air computation. The shared and separated schemes were proposed, and the accuracy of over-the-air computation was optimized by jointly designing the data transmission beamformer and the aggregation beamformer or the data beamformer and the radar sensing beamformer. In [11], the authors proposed a new waveform design based on constructive interference for the ISAC system with multiple communication users. Their results show that the proposed scheme can reduce the transmit power for the given constraint on estimation accuracy or increase the communication signal-to-noise ratio (SNR) with a given power budget. The authors in [12] investigated the SNR-constrained and CRB-constrained joint beamforming and reflection design problems for the reconfigurable intelligent surface (RIS)-aided ISAC systems. The beamforming matrix and RIS reflection

matrix were jointly optimized to maximize the sum of communication users' communication rate while considering the SNR/CRB, the BS's transmission power, and the RIS's unit-modulus constraints. In [13], the authors proposed a symbiotic sensing and communication framework composed of BS and passive sensing nodes. It considers both fully digital arrays and hybrid analog-digital (HAD) arrays, and maximized the achievable sum rate through beamforming design under the constraint of the Cramér-Rao Lower Bound (CRLB) for two-dimensional angle-of-arrival estimation. In [14], the angle and the reflection coefficient of the target and the CRB of the angle estimation were utilized as the performance metric of the point TS scenario. The authors adopted three performance metrics, the trace of CRB (TCRB), the maximum eigenvalue of CRB (MECRB), and the determinant of CRB (DCRB), respectively, to estimate the complete target response matrix with the extended TS scenario. Due to the possibility of mutual interference between the multiplexed signals, there is a trade-off between TS and communication when multi-beam transmitted signals were reused for both sensing and communications. The EE of the ISAC with an extended target and a multi-antenna communication user was investigated in [15]. The energy consumption at the transmitter with the on-off scheme was minimized by jointly designing the transmit covariance matrix and the time allocation while taking the QoS for the communication user and the CRB constraints for the target into account. In [16], two optimization problems were formulated for the full-duplex ISAC systems. The power consumption was minimized and the sum rate was maximized by jointly optimizing the downlink dual-functional transmit signal, the uplink receive beamformers at the BS, and the transmit power at the uplink users. In [17], the joint active and passive beamforming design problem for the RIS-assisted full-duplex ISAC systems with multiple communication users was considered. The sum rate was maximized by jointly optimizing the transmit beamformer, the linear postprocessing filters, the users' uplink transmission power, and the reflected phase shift of RIS. Ref. [18] investigated the joint receiver design for multiple-input multiple-output ISAC, proposing two design strategies for simultaneous symbol detection and target estimation for the radar signals received by the receiver and the signals from the uplink communication users. In [19], the authors analyzed the impact of the successive interference cancellation order on the perceived rate and communication rate in the uplink of a non-orthogonal multiple access ISAC system.

Like other wireless communication systems, ISAC systems also face security issues, and the confident signals are accessible to be wiretapped [4]. Since the transmit signals were reused for both sensing and communication, the security issue becomes imperative, especially when the target is a potential eavesdropper [20]-[26]. For the communication-centered works, the secrecy performance was optimized while taking the radar performance and other system constraints into account [20]-[23]. In [20], the radar target was assumed to be a potential eavesdropper, and the SNR at the potential eavesdropper was minimized by designing the radar beam pattern while ensuring the SINR requirement at legitimate

users (LUs). Both the scenarios with perfect/imperfect target angle and the channel state information (CSI) were considered, respectively. In [21], destructive interference was utilized to suppress the potential eavesdropper in the ISAC systems, and the SINR of the radar signals at the BS was maximized by jointly designing the transmit and receive beamforming matrices. Assuming the estimation error of the azimuth angle of the potential eavesdropper obeys the Gaussian distribution, the authors in [22] proposed a new CSI error model. Both the scenarios with the perfect eavesdropping CSI/a single LU and with imperfect eavesdropping CSI/multiple LUs were considered. The sum secrecy rate of the considered ISAC system was maximized by optimizing a beamforming vector while considering the CRB and QoS constraints. In [23], the authors investigated the secure transmission of simultaneously transmitting and reflecting (STAR)-RIS-assisted ISAC systems. The transmitted beaming, artificial jamming, and passive transmitted and reflected beam formation for STAR-RIS were jointly designed to maximize the sum secrecy rate while taking the target minimum beam pattern gain constraint into account.

For the sensing-centered works, the weighted sum of beam-pattern matching errors and cross-correlation patterns was utilized as the optimization objective to meet the practical requirements of sensing performance in different scenarios in the target tracking stage [24]-[26]. Specifically, the scenarios with perfect and imperfect CSI for the ISAC with multiple communication users and potential eavesdropper were considered in [24]. The weighted sum of the mean square error (MSE) between the designed and desired beampatterns and the mean-squared cross-correlation pattern was minimized by jointly optimizing the covariance matrix of the transmitted signals. The authors of Ref. [25] investigated the joint secure transmit beamforming designs for ISAC systems with a single LU and multiple potential eavesdroppers. The weighted sum of beampattern matching MSE and cross-correlation patterns was minimized by jointly optimizing the information and the sensing covariance matrices. The scenarios with bounded CSI errors and Gaussian CSI errors were considered, and the worst-case secrecy rate and the secrecy outage constraints were considered, respectively. In [26], the authors proposed a novel sensing-aided secure scheme for the ISAC systems to obtain the trade-off between secrecy communication and radar sensing performance. Firstly, the potential eavesdroppers' direction was estimated using the combined capon and approximate maximum likelihood technique. Then, the dual-functional beamforming and the artificial noise (AN) matrix were jointly optimized to maximize the normalized weighted sum of the secrecy rate and estimated CRB under the estimated angle errors and the system power budget constraints.

In ISAC systems, the coexisting strong radar signals can be utilized as inherent jamming signals to fight the external eavesdroppers and improve the transmission security [4]. The authors in [27] investigated the joint designs of secure transmit beamforming for ISAC systems with multiple eavesdroppers. For the scenario with the eavesdropping CSI, the maximum eavesdropping SINR of multiple eavesdroppers was minimized by jointly designing the transmit beamformers of communication and radar systems while satisfying the QoS of LUs', the

SINR constraint of radar target echo, and the transmit power budget. For the scenario without the eavesdropping CSI, an AN-aided transmit beamforming scheme was proposed. The total transmit power of the BS and radar was minimized by jointly designing the transmit beamformer and the covariance matrices of the AN vector at the BS and radar under the SINR constraints of LUs' communication and radar target echoes. In [28], an unmanned aerial vehicle (UAV) was utilized as the RIS-aided ISAC base station (BS) and a secure transmission scheme was proposed to maximize the average achievable rate or the EE by jointly designing the transmit power allocation, the scheduling of users and targets, the phase shifts at RIS, as well as the trajectory and velocity of the UAV. In [29], the authors proposed a physical layer security scheme for the rate splitting multiple access system under the constraint of sensing CRB. For the two scenarios of the eavesdropper's channel being perfect and the channel being unknown, under the premise of taking into account user fairness, the maximum energy efficiency is achieved by jointly optimizing the beam design.

Proactive eavesdropping (PE), also called wireless surveillance, is an effective method of supervising unauthorized wireless monitoring in the physical layer. To be specific, legitimate eavesdroppers wiretap the illegitimate wireless communication between transmitters and receivers to maintain public safety. Compared with traditional physical layer security (PLS), the main differences are summarized as follows [30]. 1) **Application scenarios:** In PLS scenarios, the communication between transmitters and receivers is assumed to be rightful, the eavesdroppers are illegitimate, and various schemes are designed to prevent information leakage to the malicious or potential eavesdroppers [20]-[28]. In PE scenarios, it is presumed that the eavesdroppers are legitimate and approved by government agencies to monitor the suspicious communication between transmitters and receivers, such as criminals or terrorists who may jeopardize public safety [31]-[33]. Thus, in PLS scenarios, all the efforts are from the transmitters and/or receivers, while all the works are from the view of eavesdroppers in PE scenarios. 2) **Prerequisites:** Two conditions are assumed in PE scenarios. One is that the illegitimate transmitter has the CSI of the unauthorized link, and there is an adaptive transmission between the suspicious source and the destination. The other is that the eavesdropper has global CSI and can decode unauthorized wireless information with any small error based on perfect self-interference cancellation (SIC) since the eavesdropper fully knows the transmission scheme of the illegal link as well as the encoding method [33], [34]. There are no similar assumption in PLS scenarios. 3) **Performance metric:** In PLS scenarios, the fundamental metric is the achievable secrecy rate, defined as the (non-negative) difference between the achievable rate of the communication link (R_D) and the achievable rate of the eavesdropping link (R_E). Based on secrecy rate, there are two main performance metrics: average secrecy rate and secrecy outage probability, which denote the statistical average or time average of secrecy rate and the probability that the secrecy rate falls below a target rate [20]-[28]. In PE scenarios, the relationship between R_D and R_E is crucial. When $R_E \geq R_D$, surveillance is

successful, and R_D is called the eavesdropping rate (ER). Otherwise, surveillance fails, and the ER is equal to zero [31]-[35]. For the scenarios for content analysis and event-based monitoring, there are two main performance metrics: average ER (AER) and successful eavesdropping probability (SEP), also called as eavesdropping non-interrupt probability [33], [36]. 4) **Motivation:** The motivation of PLS is to make the secrecy rate as large as possible while the aim in PE is to make R_D as large as possible under the condition $R_E \geq R_D$ [33]. In particular, when $R_E < R_D$, the eavesdropper will utilize some scheme (such as transmitting jamming signals) to ensure successful eavesdropping ($R_E \geq R_D$). In the scenarios with $R_E > R_D$, the eavesdropper will utilize some scheme (such as forwarding signals for D) to make R_D as large as possible under the condition $R_E \geq R_D$ [31], [32]. In summary, PE is an effective technology in the physical layer to maintain public safety. All the schemes utilized at upper layers, such as encryption, are out of the scope of this area.

For the PE scenarios, many works propose outstanding schemes that can be divided into two types [31]. One is spoofing relaying-based PE schemes that forward the suspicious signal to the illegitimate receivers, and the other is jamming-based PE schemes that utilize the jamming signals to control the interference at the illegitimate receivers. The spoofing relaying-based PE scheme is suitable for scenarios wherein the eavesdropping channel is of higher quality than the illegal channel. For example, the authors in Ref. [31] proposed a power splitting scheme wherein the signal received at the monitor with multiple antennas was utilized for eavesdropping and spoofing relaying, respectively. The AER was maximized by jointly designing the power splitting ratios and the precoding matrix at the monitor. With the help of an amplify-and-forward (AF) spoofing relay, a UAV was utilized to eavesdrop on multiple suspicious terrestrial links in [32]. The AER was maximized by jointly optimizing the precoder at the relay, the receive combiner at the monitor, and the UAV's trajectory.

For the scenarios wherein the quality of the illegal channel is better than that of the eavesdropping channel, jamming signals are utilized to achieve successful PE [33]. In particular, in Ref. [35], a full-duplex monitor transmits jamming signals while wiretapping illegitimate messages. The legitimate transmitter cooperated with the monitor to control the interference on the illegitimate receiver. The SEP of the multiple carrier interference network was maximized by jointly optimizing the transmit power of the eavesdropper and legitimate receiver, and an algorithm based on the Lagrange duality method was proposed to solve the formulated problem. In [36], the legitimate transmitter with multiple antennas acted as the proactive eavesdropper and utilized the intended communication signal for a legitimate receiver to affect the illegitimate receiver. The SEP of the system was maximized by jointly designing the transmitting and receiving beamformers at the full-duplex eavesdropper. In Ref. [37], two suspicious communication links were simultaneously wiretapped by a particular full-duplex monitor with multiple antennas. The achievable ER region for the minimum-MSE receivers was investigated and closed-form expressions of the upper and lower boundary points were derived. Moreover, they proposed

TABLE I: Comparison of Related Works on ISAC.

Reference	Communication metric	Sensing metric	Angle error	Optimization objectives	Main parameters	System
[20]	Eavesdropper SNR and legitimate user SINR	beam pattern matching errors/beam pattern gains	✓	Received SNR of targets	Waveform covariance matrix	Multiple users, a target potential Eve
[21]	SNR of user	Radar echo SINR		SINR of radar echo	Transmit waveform, receive beamformer	Multiple users, a point-like target
[22]	Secrecy rate	CRB	✓	Worst secrecy rate	Beamforming vector	Multiple users, a single target/Eve
[23]	Sum secrecy rate	Beam pattern gain		Sum secrecy rate	Transmit beamformer, artificial jamming vector, STAR-RIS's vectors	Multiple users, a single target
[24]	SINR of users and Eve	Beam pattern matching MSE and cross-correlation pattern		Weighted sum of beam pattern matching errors and cross-correlation patterns	Transmit beamformer	Multiple users, multiple targets
[25]	Achievable secrecy rate	Beam pattern matching MSE and cross-correlation pattern		Weighted sum of beam pattern matching errors and cross-correlation patterns	Transmit covariance matrix and the sensing/AN covariance matrix	Single user, multiple targets
[26]	Secrecy rate	CRB	✓	Weighted sum of CRB and secrecy rate	Transmit covariance matrix	Multiple users, multiple targets/Eves
[27]	Communication SINR and eavesdropping SINR	Radar output SINR		Eavesdropping SINR/transmit power	BS transmit beamformer, radar transmit beamformer, radar receive filter	Multiple eavesdroppers, multiple users
[28]	Average achievable rate	Received power		Average achievable rate	Transmit power allocation, users and target scheduling, IRS's phase shifts, trajectory and velocity of the UAV	Multiple users, multiple targets
Our work	ER	CRB	✓	SNR, CRB	Waveform covariance matrix	An illegal user, multiple targets

a time-sharing-based jamming scheme to enlarge this region by designing the transmit covariance matrix while taking the power budget into account. The authors in [38] proposed a cooperative PE scheme where the primary and assistant monitors cooperatively wiretapped multiple suspicious links. The eavesdropping EE was maximized by designing jamming power and the scheme between monitors while taking the energy transfer and load balancing constraints into account. The authors in Ref. [39] proposed a new cooperative PE scheme wherein multiple AF full-duplex relaying monitors simultaneously received and forwarded the suspicious signals to the center monitor. The AER was maximized by jointly optimizing the receive combining vector at the central monitor, the precoders at the relays and the transmit covariance matrix at the jammer. Table I outlines the typical works on ISAC.

B. Motivation and Contributions

As stated in the previous subsection, in PE scenarios wherein the quality of the eavesdropping link is weaker than that of the illegitimate communication link ($R_E < R_D$), the eavesdropper will utilize some scheme (such as transmitting AN) to ensure successful eavesdropping ($R_E \geq R_D$). Moreover, in ISAC systems, the strong radar signals have been utilized as inherent jamming signals to fight the external eavesdroppers and improve the secrecy performance of the legitimate. The above works implement communication and sensing functions within the ISAC system, but the results can not be utilized in PE scenarios because of the different motivations between the PLS and PE. Thus, we have the following questions: *How do we utilize the radar signals in PE scenarios? What is the effect of joint PE and TS?* To answer these questions, we propose two waveform design schemes: one that maximizes the ER and the other that minimizes the DCRB. Then, a normalized weighted optimization problem is formulated to optimize PE and TS jointly. *Relative to realizing the trade-off between PLS and TS in many outstanding works, such as [8], [20], [21], [23], [24], [25], [26], etc., the results*

in this work demonstrate that the proposed beamforming scheme can catch two birds (PE and TS) simultaneously.

For clarity, the contributions of this work are listed as follows.

- 1) We consider the scenario in which a multi-antenna BS actively wiretaps the illegal links while sensing multiple targets. The beam transmitted by the BS for TS is also utilized as an AN to interfere with illegal links and enable successful PE. We firstly optimize the transmitting beam of the BS only to maximize the ER or only minimize the DCRB, respectively. The semi-definite relaxation (SDR) method was employed to solve the PE and TS optimization problems after dropping the rank-one constraint.
- 2) To realize PE and TS simultaneously, the PE-centric, TS-centric, and the normalized weighted optimization problems are formulated while taking the maximum transmit power constraint into account. All the formulated problems are solved by the SDR technique and the sequential rank-one constraint relaxation (SROCR) method. Furthermore, the scenario in which the quality of the eavesdropping channel is stronger than that of the illegal channel is considered.
- 3) Relative to realizing the trade-off between PLS and TS in many outstanding works, such as [8], [20], [21], [23], [24], [25], [26], the proposed scheme can effectively realize PE and TS simultaneously. The sensing signals are utilized as AN in these works to suppress the illegitimate receivers, and in theory, the more interference to the illegitimate receivers, the better the secrecy performance. *There is a trade-off between communication and sensing performance in ISAC systems.* However, in our work, the sensing signals need to be designed carefully since excessive interference to the illegitimate receivers will result in lower ER. *To the best of the authors' knowledge, no open literature addresses the joint TS and PE optimization problem. More interestingly, the results in*

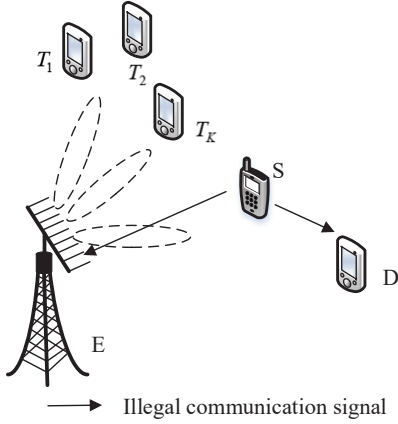


Fig. 1: System model consisting of an illegal source (S), a destination (D), K targets ($T_k, k = 1, \dots, K$) and a BS (E).

this work demonstrated that the proposed scheme can achieve a win-win in the joint TS and PE scenario.

- 4) Relative to Refs. [30]-[39] wherein the outstanding schemes (such as spoofing relaying-based and jamming-based schemes) were proposed to achieve successful PE with some additional resources (such as the relay or transmitting jamming signals), this work utilizes the existing sensing signals to achieve successful PE while completing the sensing function. Thus, more integration gain (especially EE) and coordination gain are obtained.

C. Organization

The remaining organization of this paper is summarized as follows. Sect. II introduces the system model of the joint PE and TS communication. In Sects. III and IV, the PE-centric, TS-centric, and the normalized weighted optimization problems are formulated and solved by the SDR technique and the SROCR method. In Sect. V, the simulation results of the algorithm are presented and analyzed. Finally, Sect. VI summarizes this work. TABLE II lists the notations and symbols utilized in this work.

Notations: Vectors and matrices are represented in lowercase and uppercase boldface letters, respectively, \mathbf{I} denotes an identity matrix with appropriate dimensions, $(\cdot)^{-1}$ and $(\cdot)^T$ represent the inverse and transpose of the matrix, respectively, $(\cdot)^*$ and $(\cdot)^H$ represent the conjugate and conjugate transpose of the matrix, respectively, $\text{tr}(\cdot)$ represents the trace of a matrix, $(\cdot)_{(i,j)}$ denotes the (i, j) -th element of the matrix, \odot denotes Hadamard product, and $\text{Re}(\cdot)$ and $\text{Im}(\cdot)$ signify the real and the imaginary parts of a complex-valued matrix, respectively.

II. SYSTEM MODEL

As shown in Fig. 1, we consider a joint TS and PE system which consists of a single-antenna illegal transmission source node (S), a single-antenna destination node (D), K sensing targets ($T_k, k = 1, \dots, K$), and a BS (E) equipped with uniform linear array with N_t transmitting and N_r receiving antennas. There is an illegal link for adaptive transmission between

TABLE II: List of main symbol Notations.

Notation	Description
d_{SD}	Distance between S and D
d_{SE}	Distance between S and E
d_{ED}	Distance between E and D
a_r, a_t	Steering vector of the transmitting/receiving arrays
β_k	Normalized coefficients for target reflection complex amplitude and path attenuation of target T_k
A_r, A_t	Steering matrix for multiple targets angles of the transmitting/receiving arrays
θ	Vector of multiple target angles
β	Normalized coefficients for target reflection complex amplitude and path attenuation of multiple target angles
θ_{T_k}	Azimuth of the pre-estimated target T_k
θ_D	Azimuth of D
Ω	Detection range except the target angle θ_{T_k}
Ω_1	Detection range except the mainlobe
Ω_2	Mainlobe
d	Antenna spacing
λ	Wavelength
σ_D^2, σ_E^2	Receiver noise power
σ^2	Radar noise power
β_0	Channel gain at the reference distance
α	Path loss exponent
N_t, N_r	Number of transmitting/receiving antennas
ρ	Weighting factor
φ	Scalar associated with the wide main beam fluctuation
γ_s	Requirement between the gain of the target direction and the gain of other directions
α_Φ	Threshold of the DCRB
α_I	Threshold of D ' angle beampattern gains
δ	Convergence accuracy
P_S, P_0	Transmit power of S and E

S and D [35], [36], and E transmits signals simultaneously to sense T_k and wiretap the information that S sends to D . It is assumed that the location of S and D , the CSI of S - D link, and azimuth angle of T_k are available at E ¹. The signals transmitted by E to sense T_k is also utilized as a controllable AN to achieve successful PE. Thus, the beam is designed to improve the accuracy of the estimation as well as the PE performance.

A. Target Sensing Model

The transmitted signal, $\mathbf{x}_E \in \mathbb{C}^{N_r \times 1}$, at E is expressed as

$$\mathbf{x}_E = \mathbf{w}s, \quad (1)$$

where $\mathbf{w} \in \mathbb{C}^{N_r \times 1}$ is the transmit beamforming to be designed and s denotes the symbols with unit power. The echo received

¹Note that these information can be obtained through the preceding detection and this assumption has been utilized in lots of literature focused on ISAC, such as [8], [25]. Explicitly, the location of S can be easily estimated by its transmitted signals. The locations of D and T_k can be obtained with the proposed schemes in some outstanding works on the ISAC systems, such as [8] [14], [25], [26]. The parameter estimation consists of rough estimation, waveform design, and fine estimation, which form a closed-loop optimization logic. This work focuses on waveform design, which serves as a "bridge" connecting rough and fine estimation. Based on the rough estimation results, a transmission waveform that is insensitive to errors is designed to enhance the recognizability of the target parameters in the received signal.

by the radar is expressed as²

$$\mathbf{Y}(\boldsymbol{\theta}) = \mathbf{A}_r(\boldsymbol{\theta})\boldsymbol{\beta}\mathbf{A}_t^T(\boldsymbol{\theta})\mathbf{x}_E + \mathbf{Z}, \quad (2)$$

where $\boldsymbol{\theta} = [\theta_{T_1}, \dots, \theta_{T_K}]^T$, θ_{T_k} is the angle of the k -th target wherein the first antenna is utilized as the reference point, $k = 1, \dots, K$, $\mathbf{A}_r = [\mathbf{a}_r(\theta_{T_1}), \dots, \mathbf{a}_r(\theta_{T_K})]$, $\mathbf{A}_t = [\mathbf{a}_t(\theta_{T_1}), \dots, \mathbf{a}_t(\theta_{T_K})]$, $\mathbf{a}_t(\theta_{T_k}) = [1, e^{j\frac{2\pi d}{\lambda} \sin(\theta_{T_k})}, \dots, e^{j\frac{2\pi d}{\lambda} (N_t-1) \sin(\theta_{T_k})}]^T$, $\mathbf{a}_r(\theta_{T_k}) = [1, e^{j\frac{2\pi d}{\lambda} \sin(\theta_{T_k})}, \dots, e^{j\frac{2\pi d}{\lambda} (N_r-1) \sin(\theta_{T_k})}]^T$, d is the antenna spacing, λ denotes the wavelength, $\boldsymbol{\beta} = \text{diag}([\beta_1, \dots, \beta_K]^T)$, $\beta_k = \beta_{R_k} + j\beta_{I_k}$ denotes the normalized parameter which depends on the complex amplitude of the target reflection and path loss of the $S-D$ link [6], [8], [25], $\mathbf{Z} \sim CN(0, \sigma^2 \mathbf{I})$, and σ^2 is noise power. According to (2), $\mathbf{Y}(\boldsymbol{\theta}) \sim CN(\mathbf{A}_r(\boldsymbol{\theta})\boldsymbol{\beta}\mathbf{A}_t^H(\boldsymbol{\theta})\mathbf{x}_E, \sigma^2 \mathbf{I})$.

It must be noted that, although the distance among all the nodes, and the pre-estimated azimuth angle and the reflection amplitude are available at E , the aim of TS in this work is to improve the estimation performance of azimuth and reflection amplitude information through careful design of the radar waveform. We define $\boldsymbol{\zeta} = [\boldsymbol{\theta}, \boldsymbol{\beta}_R, \boldsymbol{\beta}_I]$. Since $\sigma^2 \mathbf{I}$ is independent of the estimator [8], [26], [41], therefore, the Fisher information matrix (FIM) for $\boldsymbol{\zeta}$ is expressed as

$$\mathbf{F}(\boldsymbol{\zeta}) = \frac{2}{\sigma^2} \begin{bmatrix} \text{Re}(\mathbf{F}_{11}) & \text{Re}(\mathbf{F}_{12}) & -\text{Im}(\mathbf{F}_{12}) \\ \text{Re}^T(\mathbf{F}_{12}) & \text{Re}(\mathbf{F}_{22}) & -\text{Im}(\mathbf{F}_{22}) \\ -\text{Im}^T(\mathbf{F}_{12}) & -\text{Im}^T(\mathbf{F}_{22}) & \text{Re}(\mathbf{F}_{22}) \end{bmatrix}, \quad (3)$$

where $F_{11} = (\mathbf{A}_r^H \dot{\mathbf{A}}_r) \odot (\boldsymbol{\beta}^* \dot{\mathbf{A}}_t^H \mathbf{R}^* \mathbf{A}_t \boldsymbol{\beta}) + (\mathbf{A}_r^H \mathbf{A}_r) \odot (\boldsymbol{\beta}^* \dot{\mathbf{A}}_t^H \mathbf{R}^* \dot{\mathbf{A}}_t \boldsymbol{\beta}) + (\dot{\mathbf{A}}_r^H \dot{\mathbf{A}}_r) \odot (\boldsymbol{\beta}^* \mathbf{A}_t^H \mathbf{R}^* \mathbf{A}_t \boldsymbol{\beta}) + (\dot{\mathbf{A}}_r^H \mathbf{A}_r) \odot (\boldsymbol{\beta}^* \mathbf{A}_t^H \mathbf{R}^* \dot{\mathbf{A}}_t \boldsymbol{\beta})$, $F_{12} = (\mathbf{A}_r^H \mathbf{A}_r) \odot (\boldsymbol{\beta}^* \dot{\mathbf{A}}_t^H \mathbf{R}^* \mathbf{A}_t) + (\dot{\mathbf{A}}_r^H \mathbf{A}_r) \odot (\boldsymbol{\beta}^* \mathbf{A}_t^H \mathbf{R}^* \mathbf{A}_t)$, $F_{22} = (\mathbf{A}_r^H \mathbf{A}_r) \odot (\mathbf{A}_t^H \mathbf{R}^* \mathbf{A}_t)$, $\dot{\mathbf{A}}_r = \left[\frac{\partial \mathbf{a}_r(\theta_{T_1})}{\partial \theta_{T_1}}, \dots, \frac{\partial \mathbf{a}_r(\theta_{T_K})}{\partial \theta_{T_K}} \right]$, $\dot{\mathbf{A}}_t = \left[\frac{\partial \mathbf{a}_t(\theta_{T_1})}{\partial \theta_{T_1}}, \dots, \frac{\partial \mathbf{a}_t(\theta_{T_K})}{\partial \theta_{T_K}} \right]$, and $\mathbf{R} = \mathbf{w}\mathbf{w}^H$.

Proof. *Proof:* See the Appendix A. \square

The CRB matrix is obtained as

$$\boldsymbol{\Phi}(\boldsymbol{\zeta}) = (\mathbf{F}(\boldsymbol{\zeta}))^{-1}. \quad (4)$$

² Like [16], [27], since the radar host generally has a strong signal separation capability, and a variety of methods can be used for filtering, E is assumed to perfectly separate the signal (the echo from S) from the interference (the echo from D). It should be noted that this is called the worst-case scenario for PLS [40] but is the best-case scenario for PE since this assumption overestimates the eavesdropper's decode-ability in many scenarios.

B. Proactive Eavesdropping Model

It is assumed that the link between E and D is line-of-sight³ and the channel coefficient is expressed as [22]

$$\mathbf{h}_{ED} = \sqrt{\frac{\beta_0}{d_{ED}^\alpha}} \mathbf{a}_t(\theta_D), \quad (5)$$

where β_0 represents the channel gain at the reference distance, d_{ED} represents the distance between E and D , α denotes the path loss exponent, and θ_D denotes the angle of D . Similarly, the channel coefficient between S and D is expressed as

$$h_{SD} = \sqrt{\frac{\beta_0}{d_{SD}^\alpha}}, \quad (6)$$

where d_{SD} represents the distance between S and D . The received signal at D is expressed as

$$y_D = h_{SD} x_S + \mathbf{h}_{ED}^H \mathbf{x}_E + n_D, \quad (7)$$

where x_S denotes the signal sent by S , and $n_D \sim N(0, \sigma_D^2)$ is the Additive White Gaussian Noise. The SINR of received signal at D is expressed as

$$\gamma_D = \frac{\beta_0 d_{SD}^{-\alpha} P_S}{\beta_0 d_{ED}^{-\alpha} I(\theta_D) + \sigma_D^2}, \quad (8)$$

where P_S is the transmit power of S and $I(\theta_D) = \mathbf{a}_t^H(\theta_D) \mathbf{R} \mathbf{a}_t(\theta_D)$ signifies the beampattern gains at D from E .

The communication signals received at E is expressed as

$$\mathbf{y}_E = \mathbf{h}_{SE} x_S + \mathbf{n}_E, \quad (9)$$

where $\mathbf{n}_E \sim N(0, \sigma_E^2 \mathbf{I})$, $\mathbf{h}_{SE} \in \mathbb{C}^{N_r \times 1}$ is the $S-E$ channel. It is assumed that E adopts the selection combining scheme, the SNR of E is expressed as

$$\gamma_E = \frac{P_S |h_{SE}|^2}{\sigma_E^2}, \quad (10)$$

where $h_{SE} = \sqrt{\frac{\beta_0}{d_{SE}^\alpha}}$ and d_{SE} represents the distance between S and E .

III. PROBLEM FORMULATION

In this section, we design the covariance matrix for PE and TS, respectively, to lay the foundation for optimizing the performance of PE and TS at the same time.

³ This work assumes the link between E and D is line-of-sight and the CSI is perfectly known. It is easy to extend the results to scenarios with small-scale fading and/or with imperfect CSI. For the scenarios where there is a non-line-of-sight link between the transmitter and receiver, the channel gains can be approximated by their expectation by utilizing Jensen's inequality, like Refs. [29], [42] and [43]. For the bounded CSI error model, the distance between E and T_k/D can be approximated by its upper bound, which can be obtained based on the triangle inequality [43]. For the Gaussian CSI error model, the distances can be approximated by its expectation.

A. Proactive Eavesdropping Only

It is assumed that there is an adaptive information transmission link between S and D , E can decode the received information without error, and the success of PE needs to meet $\gamma_D \leq \gamma_E$ [35], [36]. In this subsection, the transmitting beam is designed only to meet the eavesdropping demand. To maximize the ER on the premise of successful PE, the following optimization problem is formulated

$$\mathcal{P}_1 : \max_{\mathbf{R}} \log_2(1 + \gamma_D) \quad (11a)$$

$$\text{s.t. } \text{tr}(\mathbf{R}) \leq P_0, \quad (11a)$$

$$\mathbf{R} \geq 0, \quad (11b)$$

$$\text{rank}(\mathbf{R}) = 1, \quad (11c)$$

$$\gamma_D \leq \gamma_E, \quad (11d)$$

where (11a) is the constraint on total power with the maximum allowable power budget P_0 of E , (11b) indicates that the covariance matrix \mathbf{R} is a positive semi-definite matrix, (11c) indicates that the rank of \mathbf{R} is one, and (11d) is the premise of successful eavesdropping. Based on (8) and (10), (11d) is rewritten as⁴

$$\frac{d_{ED}^\alpha}{\beta_0} \left(\frac{h_{SD}^2 \sigma_E^2}{h_{SE}^2} - \sigma_D^2 \right) \leq \mathcal{I}(\theta_D). \quad (12)$$

Moreover, it is easily found that maximizing ER equals minimizing $\mathcal{I}(\theta_D)$, then, \mathcal{P}_1 is equivalent to

$$\mathcal{P}_{1.1} : \min_{\mathbf{R}} \mathcal{I}(\theta_D) \quad (13a)$$

$$\text{s.t. } \text{tr}(\mathbf{R}) \leq P_0, \quad (13a)$$

$$\mathbf{R} \geq 0, \quad (13b)$$

$$\text{rank}(\mathbf{R}) = 1, \quad (13c)$$

$$\frac{d_{ED}^\alpha}{\beta_0} \left(\frac{h_{SD}^2 \sigma_E^2}{h_{SE}^2} - \sigma_D^2 \right) \leq \mathcal{I}(\theta_D). \quad (13d)$$

$\mathcal{P}_{1.1}$ is challenging to solve because (13c) is non-convex. Fortunately, with the proposed method in [20], $\mathcal{P}_{1.1}$ can be solved directly by the convex optimization toolbox by ignoring (13c).

B. Target Sensing Only

CRB is the lower bound of the unbiased estimation variance, and therefore minimizing CRB is a strategy for improving the accuracy of the estimation⁵. In this subsection, the transmitting beam is designed only to minimize the DCRB.

⁴It is unnecessary for E to send AN to D when the channel quality of $S-E$ is better than that of $S-D$, i.e. $\frac{h_{SD}^2}{\sigma_D^2} \leq \frac{h_{SE}^2}{\sigma_E^2}$ [44]. The ER is maximized only if the interference in the D 's direction is zero, in particular, $\mathcal{I}(\theta_D) = 0$. Here we mainly consider the normal case where $\frac{h_{SD}^2}{\sigma_D^2} > \frac{h_{SE}^2}{\sigma_E^2}$.

⁵ There are three different types of scalar CRB metrics: TCRB, MECRB, and DCRB [14], [41]. To comprehensively evaluate the joint estimation performance of multiple parameters, the DCRB should be prioritized. If a quick comparison of independent estimation accuracy for individual parameters is needed, the TCRB is the preferred choice. For ensuring controllable estimation error under worst-case conditions, the MECRB should be given priority. In this work, the DCRB is chosen as the performance metric of TS. The proposed schemes in this work also fit those scenarios wherein the trace and the maximum eigenvalue of the CRB are utilized as the matrices.

1) *Perfect Target Direction*: When the given target angle is perfect, the formulated problem is expressed as

$$\mathcal{P}_{2.1} : \min_{\mathbf{R}} |\Phi(\zeta)| \quad (14a)$$

$$\text{s.t. } \text{tr}(\mathbf{R}) \leq P_0, \quad (14a)$$

$$\mathbf{R} \geq 0, \quad (14b)$$

$$\text{rank}(\mathbf{R}) = 1, \quad (14c)$$

$$\mathcal{I}(\theta_{T_k}) - \mathcal{I}(\theta_n) \geq \gamma_s, \forall \theta_n \in \Omega, \forall k, \quad (14d)$$

where θ_{T_k} denotes the direction of T_k , θ_n prescribes the sidelobe region, the left-hand side (LHS) of (14d) is the difference between the gain of the target direction and the gain of other directions, Ω represents the angles in the detection range except the target angle θ_{T_k} , and γ_s is the requirement between the gain of the target direction and the gain of other directions. The purpose of (14d) is to ensure that the gain in the target direction is superior to that in the other directions. $\mathcal{P}_{2.1}$ is a standard SDR problem and can be solved by CVX toolbox after ignoring the rank-one constraint.

2) *Imperfect Target Direction*: In this subsection, a more practical scenario is considered wherein the estimated target angle θ_{T_k} is imperfect and there is an uncertain angle $\Delta\theta$. Specifically, the angle of the k -th target varies in $\Omega_1 = [\theta_{T_k} - \Delta\theta, \theta_{T_k} + \Delta\theta]$. Then, the following optimization problem is formulated

$$\mathcal{P}_{2.2} : \min_{\mathbf{R}} |\Phi(\zeta)| \quad (15a)$$

$$\text{s.t. } \text{tr}(\mathbf{R}) \leq P_0, \quad (15a)$$

$$\mathbf{R} \geq 0, \quad (15b)$$

$$\text{rank}(\mathbf{R}) = 1, \quad (15c)$$

$$\mathcal{I}(\theta_{T_k}) - \mathcal{I}(\theta_n) \geq \gamma_s, \forall \theta_n \in \Omega_2, \quad (15d)$$

$$\mathcal{I}(\theta_m) \leq (1 + \varphi) \mathcal{I}(\theta_{T_k}), \forall \theta_m \in \Omega_1, \quad (15e)$$

$$\mathcal{I}(\theta_m) \geq (1 - \varphi) \mathcal{I}(\theta_{T_k}), \forall \theta_m \in \Omega_1, \quad (15f)$$

where Ω_2 represents other angles except the mainlobe and $0 \leq \varphi \leq 1$ is a given scalar associated with the wide main beam fluctuation [26], (15d) represents the gain gap constraint between the target direction and side lobes, (15e) and (15f) are both stable mainlobe gain intervals to prevent a large gain difference which affects the detection performance. $\mathcal{P}_{2.2}$ can be solved by CVX after ignoring (15c).

IV. JOINTLY OPTIMIZATION OF PROACTIVE EAVESDROPPING AND TS

Notice that in the considered system, the transmitted sensing signal is utilized as AN to interfere with the illegitimate receivers, like the works on PLS of the ISAC systems [8], [20], [21], [23], [24], [25], [26]. In these outstanding works, the more interference the illegitimate receivers, the better the secrecy performance. However, in our work, the sensing signals need to be designed carefully. Too weak interference to the illegitimate receivers will result in the failure of PE, while excessive interference to the illegitimate receivers will result in lower eavesdropping rates. Based on the problems formulated in Section III, the PE-CRB region characterizes

the achievable region for the target parameter estimation and PE is defined as

$$\mathbb{P}\mathcal{S} = \bigcup_{\mathbf{R} \geq 0} \{ \log_2(1 + \gamma_D), |\Phi(\zeta)|, |\gamma_D < \gamma_E, |\Phi(\zeta)| \leq \alpha_\Phi \}, \quad (16)$$

where α_Φ denotes the target threshold for DCRB.

A. Proactive Eavesdropping-centric Design

Firstly, the transmit covariance matrix is optimized to minimize the beampattern gains at D while ensuring a target threshold for the estimation CRB for multi-target constraint into account (called as PE-centric design). Based on $\mathcal{P}_{1.1}$, the optimization problem is formulated as

$$\mathcal{P}_3 : \min_{\mathbf{R}} I(\theta_D) \quad (17a)$$

$$\text{s.t. } \text{tr}(\mathbf{R}) \leq P_0, \quad (17a)$$

$$\mathbf{R} \geq 0, \quad (17b)$$

$$\text{rank}(\mathbf{R}) = 1, \quad (17c)$$

$$\frac{d_{ED}^\alpha}{\beta_0} \left(\frac{h_{SD}^2 \sigma_E^2}{h_{SE}^2} - \sigma_D^2 \right) \leq I(\theta_D), \quad (17d)$$

$$|\Phi(\zeta)| \leq \alpha_\Phi, \quad (17e)$$

where (17e) is the TS constraint. \mathcal{P}_3 is a convex problem after dropping constraint (17c), which can be solved by CVX toolbox.

B. Target Sensing-centric Design

Then, we consider optimizing the transmit covariance matrix to minimize the estimation CRB while ensuring a beam-pattern gains (interference) at D while taking the maximum transmit power constraint into account (called as TS-centric design). Based on $\mathcal{P}_{2.1}$ and $\mathcal{P}_{2.2}$, the optimization problem is formulated as

$$\mathcal{P}_{4.1} : \min_{\mathbf{R}} |\Phi(\zeta)| \quad (18a)$$

$$\text{s.t. } \text{tr}(\mathbf{R}) \leq P_0, \quad (18a)$$

$$\mathbf{R} \geq 0, \quad (18b)$$

$$\text{rank}(\mathbf{R}) = 1, \quad (18c)$$

$$I(\theta_{T_k}) - I(\theta_n) \geq \gamma_s, \forall \theta_n \in \Omega, \quad (18d)$$

$$\frac{d_{ED}^\alpha}{\beta_0} \left(\frac{h_{SD}^2 \sigma_E^2}{h_{SE}^2} - \sigma_D^2 \right) \leq I(\theta_D) \quad (18e)$$

$$I(\theta_D) \leq \alpha_I, \quad (18f)$$

$$\mathcal{P}_{4.2} : \min_{\mathbf{R}} |\Phi(\zeta)| \quad (19a)$$

$$\text{s.t. } \text{tr}(\mathbf{R}) \leq P_0, \quad (19a)$$

$$\mathbf{R} \geq 0, \quad (19b)$$

$$\text{rank}(\mathbf{R}) = 1, \quad (19c)$$

$$I(\theta_{T_k}) - I(\theta_n) \geq \gamma_s, \forall \theta_n \in \Omega_2, \quad (19d)$$

$$\frac{d_{ED}^\alpha}{\beta_0} \left(\frac{h_{SD}^2 \sigma_E^2}{h_{SE}^2} - \sigma_D^2 \right) \leq I(\theta_D) \quad (19e)$$

$$I(\theta_D) \leq \alpha_I, \quad (19f)$$

$$I(\theta_m) \leq (1 + \varphi) I(\theta_{T_k}), \forall \theta_m \in \Omega_1, \quad (19g)$$

$$I(\theta_m) \geq (1 - \varphi) I(\theta_{T_k}), \forall \theta_m \in \Omega_1, \quad (19h)$$

where α_I denotes the interference threshold at D . It must be noted that (18f) and (19f) denote the requirement for the ER. Obviously, α_I has an essential effect on the optimized results. $\mathcal{P}_{4.1}$ and $\mathcal{P}_{4.2}$ can be transformed into a convex problem by means of SDR and are solved directly using the CVX toolbox when (18c) and (19c) are omitted.

C. Normalized Weighted Optimization of PE and Target Sensing.

In this subsection, a normalized weighted optimization problem that simultaneously considers both PE and TS performance is proposed. Design of the weighted optimization between the DCRB and ER presents the challenge that both performance metrics have different units and potentially different magnitudes. Inspired by [26], both $I(\theta_D)$ and $|\Phi(\zeta)|$ are normalized with their respective bound obtained in $\mathcal{P}_{1.1}$ and $\mathcal{P}_{2.1}$, respectively.

1) *Joint Optimization Proactive Eavesdropping and Target Sensing*: To simultaneously consider PE and TS, while taking the uncertain angle of T_k into account, the weighted optimization problem is formulated as⁶

$$\mathcal{P}_{5.1} : \min_{\mathbf{R}} \rho \frac{I(\theta_D)}{\tilde{I}} + (1 - \rho) \frac{|\Phi(\zeta)|}{|\tilde{\Phi}|} \quad (20a)$$

$$\text{s.t. } \text{tr}(\mathbf{R}) \leq P_0, \quad (20a)$$

$$\mathbf{R} \geq 0, \quad (20b)$$

$$\text{rank}(\mathbf{R}) = 1, \quad (20c)$$

$$\frac{d_{ED}^\alpha}{\beta_0} \left(\frac{h_{SD}^2 \sigma_E^2}{h_{SE}^2} - \sigma_D^2 \right) \leq I(\theta_D), \quad (20d)$$

$$I(\theta_{T_k}) - I(\theta_n) \geq \gamma_s, \forall \theta_n \in \Omega_2, \quad (20e)$$

$$I(\theta_m) \leq (1 + \varphi) I(\theta_{T_k}), \forall \theta_m \in \Omega_1, \quad (20f)$$

$$I(\theta_m) \geq (1 - \varphi) I(\theta_{T_k}), \forall \theta_m \in \Omega_1, \quad (20g)$$

$$|\Phi(\zeta)| \leq \alpha_\Phi, \quad (20h)$$

$$I(\theta_D) \leq \alpha_I, \quad (20i)$$

where \tilde{I} and $\tilde{\Phi}$ are the results of $\mathcal{P}_{1.1}$ and $\mathcal{P}_{2.1}$ ($\mathcal{P}_{2.2}$), respectively, and $0 \leq \rho \leq 1$ signifies the weights factor

⁶ It should be noted that (20h) and (20i) correspond to $\rho = 1$ and $\rho = 0$, respectively. In particular, $\mathcal{P}_{5.1}$ degenerates into \mathcal{P}_3 and $\mathcal{P}_{4.2}$ when $\rho = 1$ and $\rho = 0$, respectively.

Algorithm 1: Joint Optimization of TS and PE without Rank-one Constraint

Input: Initialize P_0 , $\Delta\theta$, φ , γ_s , γ_D , and γ_E .
if $\gamma_D > \gamma_E$ **then**
 Solve $\mathcal{P}_{1.1}$ for given parameters and obtain the solution $\tilde{I}(\theta_D)$.
 Solve $\mathcal{P}_{2.1}$ for given parameters and obtain the solution $|\tilde{\Phi}|$.
 Solve $\mathcal{P}_{5.1}$ for the given parameters and obtain the solution.
end
else
 Solve $\mathcal{P}_{5.2}$ for the given parameters and obtain the solution.
end
Output: The covariance matrix \mathbf{R} of E .

between PE and TS. $\mathcal{P}_{5.1}$ is an SDR problem by neglecting (20e) and can be solved with the CVX toolbox.

2) *The interference power is zero:* It is unnecessary for E to send AN to D when the channel quality of $S-E$ is better than that of $S-D$, i.e. $\frac{h_{SD}^2}{\sigma_D^2} \leq \frac{h_{SE}^2}{\sigma_E^2}$ in (20d) [44]. In these scenarios, the ER is equal to the receiving rate of D without interference and \mathcal{P}_3 is transformed into a TS sub-problem, which is expressed as

$$\mathcal{P}_{5.2} : \min_{\mathbf{R}} |\Phi(\zeta)|$$

$$\text{s.t. } \text{tr}(\mathbf{R}) \leq P_0, \quad (21a)$$

$$\mathbf{R} \geq 0, \quad (21b)$$

$$\text{rank}(\mathbf{R}) = 1, \quad (21c)$$

$$I(\theta_D) = 0, \quad (21d)$$

$$I(\theta_{T_k}) - I(\theta_n) \geq \gamma_s, \forall \theta_n \in \Omega_2, \quad (21e)$$

$$I(\theta_m) \leq (1 + \varphi) I(\theta_{T_k}), \forall \theta_m \in \Omega_1, \quad (21f)$$

$$I(\theta_m) \geq (1 - \varphi) I(\theta_{T_k}), \forall \theta_m \in \Omega_1, \quad (21g)$$

where (21d) denotes the interference from E at D equal to zero. $\mathcal{P}_{5.2}$ is a standard convex problem when (21c) is omitted, which can be solved directly by CVX. The solving process of $\mathcal{P}_{5.1}$ ($\mathcal{P}_{5.2}$) ignoring rank-one constraint is summarized as **Algorithm 1**.

D. Rank-one Constraint

The rank-one constraint is non-convex, which means the relevant toolbox can not directly solve the optimization problem. The above issues are solved by omitting the rank-one constraint and the rank of the obtained solution may be larger than one. Based on Refs. [20], [26], [45], the feasible suboptimal solution of the original problem is obtained by utilizing specific methods based on the SDR technology, and rank-one constraint is solved by Gaussian randomization, singular value decomposition, etc. It must be noted that these methods may result in a certain degree of distortion, which is tolerable in many cases. However, these methods cannot be utilized to solve the previously formulated problems since the recovered result may not satisfy $\gamma_D \leq \gamma_E$, which

results in eavesdropping failure. In this work, an iterative method, SROCR, is utilized to solve this problem [46], [47]. Specifically, the rank-one constraint is relaxed by restricting the ratio of the maximum eigenvalue and trace of the matrix. In particular, for the scenario with $\text{rank}(\tilde{\mathbf{R}}) > 1$, the eigenvalue decomposition of the matrix is firstly carried out and the eigenvalue matrix $\tilde{\Sigma} = \text{diag}(\lambda_1, \dots, \lambda_{N_t})$ is obtained. According to the relationship between the matrix eigenvalue and the matrix trace, the maximum eigenvalue of $\tilde{\mathbf{R}}$ must be less than the trace. The eigenvector of maximum eigenvalue of $\tilde{\mathbf{R}}$ is expressed as \mathbf{u} and there must be $\mathbf{u}^H \tilde{\mathbf{R}} \mathbf{u} < \text{tr}(\tilde{\mathbf{R}})$. By using the iterative method, the one constraint is transformed into

$$\mathbf{u}^{(j)H} \mathbf{R} \mathbf{u}^{(j)} \geq w^{(j)} \text{tr}(\mathbf{R}), \quad (22)$$

where $(\cdot)^{(j)}$ denotes j -th iteration value and $w \in [0, 1]$ is the relaxation parameter.

Then $\mathcal{P}_{5.1}$ and $\mathcal{P}_{5.2}$ are reformulated as

$$\mathcal{P}_{5.1b} : \min_{\mathbf{R}} \rho \frac{I(\theta_D)}{\tilde{I}} + (1 - \rho) \frac{|\Phi(\zeta)|}{|\tilde{\Phi}|}$$

$$\text{s.t. } \text{tr}(\mathbf{R}) \leq P_0, \quad (23a)$$

$$\mathbf{R} \geq 0, \quad (23b)$$

$$\mathbf{u}^{(j)H} \mathbf{R} \mathbf{u}^{(j)} \geq w^{(j)} \text{tr}(\mathbf{R}), \quad (23c)$$

$$\frac{d_{ED}^\alpha}{\beta_0} \left(\frac{h_{SD}^2 \sigma_E^2}{h_{SE}^2} - \sigma_D^2 \right) \leq I(\theta_D) \quad (23d)$$

$$I(\theta_{T_k}) - I(\theta_n) \geq \gamma_s, \forall \theta_n \in \Omega_2, \quad (23e)$$

$$I(\theta_m) \leq (1 + \varphi) I(\theta_{T_k}), \forall \theta_m \in \Omega_1, \quad (23f)$$

$$I(\theta_m) \geq (1 - \varphi) I(\theta_{T_k}), \forall \theta_m \in \Omega_1, \quad (23g)$$

$$|\Phi(\zeta)| \leq \alpha_\Phi, \quad (23h)$$

$$I(\theta_D) \leq \alpha_I, \quad (23i)$$

and

$$\mathcal{P}_{5.2b} : \min_{\mathbf{R}} |\Phi(\zeta)|$$

$$\text{s.t. } \text{tr}(\mathbf{R}) \leq P_0, \quad (24a)$$

$$\mathbf{R} \geq 0, \quad (24b)$$

$$\mathbf{u}^{(j)H} \mathbf{R} \mathbf{u}^{(j)} \geq w^{(j)} \text{tr}(\mathbf{R}), \quad (24c)$$

$$I(\theta_D) = 0, \quad (24d)$$

$$I(\theta_{T_k}) - I(\theta_n) \geq \gamma_s, \forall \theta_n \in \Omega_2, \quad (24e)$$

$$I(\theta_m) \leq (1 + \varphi) I(\theta_{T_k}), \forall \theta_m \in \Omega_1, \quad (24f)$$

$$I(\theta_m) \geq (1 - \varphi) I(\theta_{T_k}), \forall \theta_m \in \Omega_1, \quad (24g)$$

respectively, where $w^{(0)} = \frac{\mathbf{u}^H \tilde{\mathbf{R}} \mathbf{u}}{\text{tr}(\tilde{\mathbf{R}})} \in [0, 1]$ and $\tilde{\mathbf{R}}$ is obtained by solving $\mathcal{P}_{5.1}$ ($\mathcal{P}_{5.2}$). The optimal result of $\mathcal{P}_{5.1b}$ ($\mathcal{P}_{5.2b}$) is denoted as $opt^{(j)}$ in the j -th iteration, which are solved by an iterative algorithm summarized as **Algorithm 2**, where θ denotes the predetermined accuracy. After obtain \mathbf{R} by solving $\mathcal{P}_{5.1b}$ ($\mathcal{P}_{5.2b}$), the beamforming vector, \mathbf{w} , is obtained through the eigenvalue decomposition.

E. Comparison of formulated problems

In this work, there are eight (two kinds of) formulated problems, which are introduced as follows.

Algorithm 2: Iterative Procedure of $\mathcal{P}_{5.1}$ ($\mathcal{P}_{5.2b}$) with Rank-one Constraint

Input: Initialize P_0 , $\Delta\theta$, φ , γ_s , γ_D, γ_E , τ , and ϑ .

$j \leftarrow 0$.

Solve $\mathcal{P}_{5.1}$ ($\mathcal{P}_{5.2}$) and obtain \mathbf{R} .

$w^{(0)} \leftarrow \frac{\mathbf{u}^H \mathbf{R} \mathbf{u}}{\text{tr}(\mathbf{R})}$.

$\delta^{(0)} \leftarrow \max \left[0, 1 - \frac{\mathbf{u}^H \mathbf{R} \mathbf{u}}{\text{tr}(\mathbf{R})} \right]$.

while $\|opt^{(j+1)} - opt^{(j)}\| \geq \vartheta$ and $w^{(j)} \leq \tau$ **do**

 Solve $\mathcal{P}_{5.1b}$ ($\mathcal{P}_{5.2b}$).

if $\mathcal{P}_{5.1b}$ ($\mathcal{P}_{5.2b}$) is solvable **then**

$\mathbf{R}^{(j+1)}$ and $\delta^{(j+1)} = \delta^{(j)}$.

end

else

$\mathbf{R}^{(j+1)} = \mathbf{R}^{(j)}$ and $\delta^{(j+1)} = \frac{1}{2} \delta^{(j)}$.

end

$w^{(j+1)} \leftarrow \min \left(\frac{\mathbf{u}^{(j+1)H} \mathbf{R}^{(j+1)} \mathbf{u}^{(j+1)}}{\text{tr}(\mathbf{R}^{(j+1)})} + \delta^{(j+1)}, 1 \right)$.

$j \leftarrow j + 1$.

end

Output: $\mathbf{R}^{(j)}$

- The first kind of problem is considering PE or TS, respectively.

- 1) In \mathcal{P}_1 ($\mathcal{P}_{1.1}$), the transmitting beam is designed only to maximize the ER, considering successful PE, and the TS is not considered.
- 2) In $\mathcal{P}_{2.1}$ and $\mathcal{P}_{2.2}$, the transmitting beam is designed only to minimize the DCRB and the PE is not considered. $\mathcal{P}_{2.1}$ assumes that the azimuth angles of targets (θ_{T_k}) are perfect, while $\mathcal{P}_{2.2}$ examines the imperfect θ_{T_k} .
- 3) The solutions of \mathcal{P}_1 and $\mathcal{P}_{2.2}$ are utilized in $\mathcal{P}_{5.1}$ and $\mathcal{P}_{5.2}$.

- The second kind of problem is considering PE and TS simultaneously.

- 1) In \mathcal{P}_3 , the transmit covariance matrix is optimized to maximize the PE performance (minimize the beam-pattern gains at D) while taking the TS constraint into account, which is called PE-centric (PEC) design.
- 2) In $\mathcal{P}_{4.1}$ and $\mathcal{P}_{4.2}$, the transmit covariance matrix is optimized to maximize the TS performance (minimize the estimation DCRB) while ensuring successful PE and ER constraints, which is called the TS-centric (TSC) design. $\mathcal{P}_{4.1}$ assumes that the azimuth angles of targets (θ_{T_k}) are perfect, while $\mathcal{P}_{4.2}$ examines the imperfect θ_{T_k} .
- 3) In $\mathcal{P}_{5.1}$ and $\mathcal{P}_{5.2}$, the normalized weighted summation between $|\Phi(\zeta)|$ and $I(\theta_D)$ is minimized considering successfully PE, DCRB requirements, and interference requirement at D , which is called as joint optimization of PE and TS (JPT) design. Different from $\mathcal{P}_{5.1}$, $\mathcal{P}_{5.2}$ considers a special scenario wherein the channel quality of $S-E$ is better than that of $S-D$, i.e. $\frac{h_{SD}^2}{\sigma_D^2} \leq \frac{h_{SE}^2}{\sigma_E^2}$. In this case, E does not need to send AN to D , and all the power

TABLE III: Comparison of formulated problems.

Problem	PE	TS	Perfect/imperfect Target Direction	$\frac{h_{SD}^2}{\sigma_D^2} \leq \frac{h_{SE}^2}{\sigma_E^2}$
\mathcal{P}_1 ($\mathcal{P}_{1.1}$)	✓			
$\mathcal{P}_{2.1}$		✓	Perfect	
$\mathcal{P}_{2.2}$		✓	Imperfect	
\mathcal{P}_3	✓	Constraint		
$\mathcal{P}_{4.1}$	Constraint	✓	Perfect	
$\mathcal{P}_{4.2}$	Constraint	✓	Imperfect	
$\mathcal{P}_{5.1}$ ($\mathcal{P}_{5.1b}$)	✓	✓	Imperfect	
$\mathcal{P}_{5.2}$ ($\mathcal{P}_{5.2b}$)	✓	✓	Imperfect	✓

can be utilized to TS.

Table III summarizes the difference for all the formulated problems.

F. Convergence Discussion and Complexity Analysis

While optimization problems involving multi-variable coupling often necessitate iterative approaches such as BCD or SCA. The convergence analysis serves as key theoretical validation. This work formulates problems containing only a single variable, \mathbf{R} . By applying SDR to relax the rank-one constraint, the problem is transformed into a convex optimization task that can be solved directly. Although this relaxation reduces computational complexity, it may introduce a performance gap between the relaxed solution and the true optimum of the original non-convex problem. To mitigate this gap and enhance solution tightness, we utilize an iterative optimization method based on rank-one relaxation. Specifically, we define the ratio of the maximum eigenvalue to the matrix trace as a relaxation performance metric and adopt a binary search strategy to refine the solution while ensuring constraint feasibility iteratively. Crucially, this approach guarantees strict improvement in the relaxation metric with each iteration. By setting a convergence threshold (e.g., 0.999), the final solution's performance index is driven arbitrarily close to 1, achieving a high-precision approximation of the original problem's optimum. This method not only circumvents the computational challenges of directly solving non-convex problems but also significantly improves accuracy through iterative refinement, offering a practical and theoretically grounded solution pathway for rank-one-constrained non-convex optimization.

The algorithm complexity analysis is as follows. $\mathcal{P}_{1.1}$ is composed of 1 linear matrix inequality (LMI) constraint of size N_t and 2 LMI constraints of size 1, the computational complexity is $O(\sqrt{N_t+2} [N_t^2 (N_t^3+2) + N_t^4 (N_t^2+2) + N_t^6])$. $\mathcal{P}_{2.2}$ is composed by 1 LMI constraints of size N_t , $2K\varpi_1 + K\varpi_2 + 1$ LMI constraints of size 1, the computational complexity is $O(\sqrt{N_t + (2K\varpi_1 + K\varpi_2 + 1)} [N_t^2 (N_t^3 + 2K\varpi_1 + K\varpi_2 + 1) + N_t^4 (N_t^2 + 2K\varpi_1 + K\varpi_2 + 1) + N_t^6])$, where ϖ_1 and ϖ_2 are cardinality of Ω_1 and Ω_2 , respectively. $\mathcal{P}_{5.1}$ have 1 LMI constraints of size N_t , $2K\varpi_1 + K\varpi_2 + 4$ LMI constraint of size 1, $\mathcal{P}_{5.2}$ have 1 LMI constraints of size N_t , $2K\varpi_1 + K\varpi_2 + 2$ LMI constraint of size 1, $\mathcal{P}_{5.1b}$ have 1 LMI constraints of size N_t , $2K\varpi_1 + K\varpi_2 + 5$ LMI constraint of size 1, $\mathcal{P}_{5.2b}$ have 1 LMI constraints of size N_t , $2K\varpi_1 + K\varpi_2 + 3$ LMI constraint of size 1. With the given

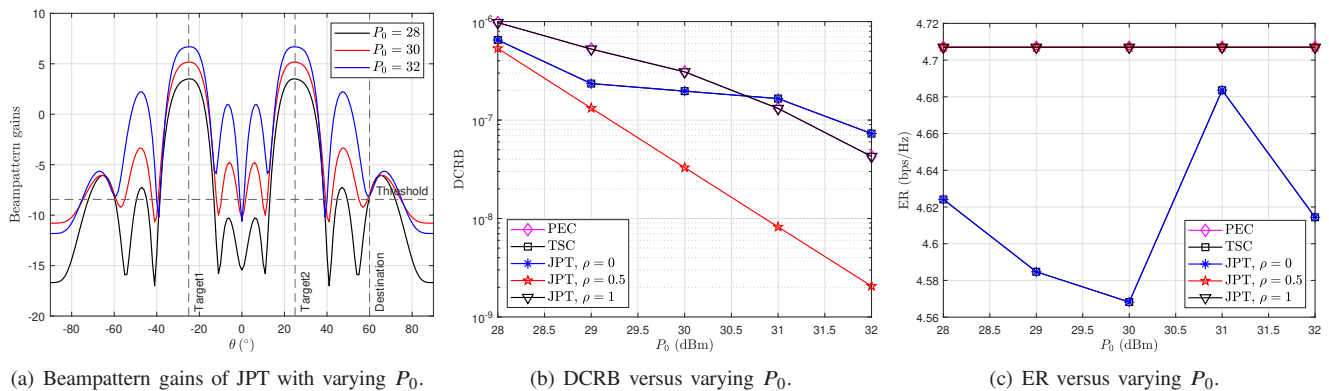


Fig. 2: The results versus varying P_0 with $N_t = 12$ and $\Delta\theta = 3$.

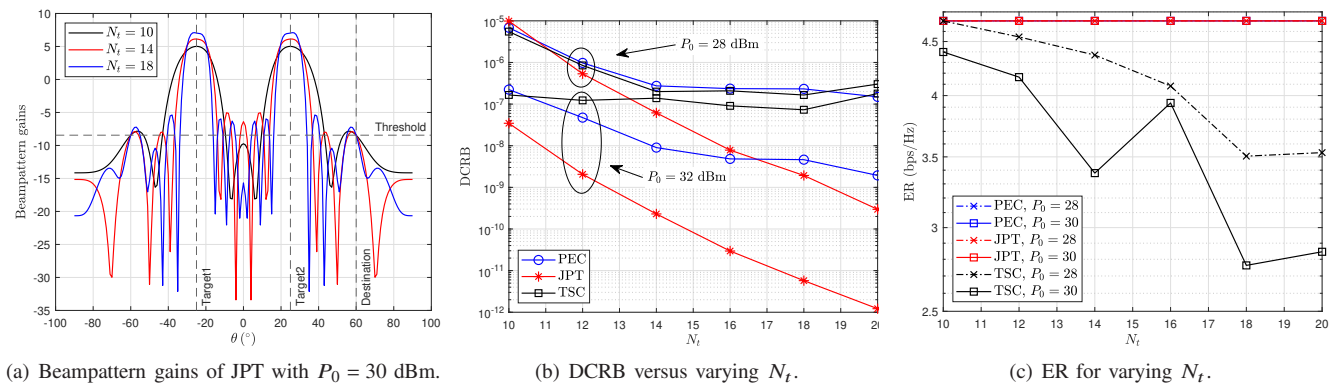


Fig. 3: The results versus varying N_t with $\rho = 0.5$ and $\Delta\theta = 3$.

TABLE IV: Parameters Setting

Parameters	Value	Parameters	Value
d_{SD}	500 m	d_{SE}	1000 m
d_{ED}	1000 m	θ_T	$-25^\circ/25^\circ$
θ_D	60°	β_0	-30 dB
λ	0.06 m	d	0.03 m
$\sigma_D^2 = \sigma_E^2$	-80 dBm	φ	0.05
γ_s	0.1	α	2.2
P_S	30 dBm	ϑ	10^{-4}
τ	0.999	$N_r = N_t$	12
α_Φ	10^{-5}	α_I	0.2

convergence accuracy ϑ , the computational complexity of algorithm 1 is expressed as $O\left(\sqrt{N_t + 2K\varpi_1 + K\varpi_2}N_t^6 \log\left(\frac{1}{\vartheta}\right)\right)$ [21], [26], the computational complexity of algorithm 2 is $O\left(I_{\text{iter}}\left(\sqrt{N_t + 2K\varpi_1 + K\varpi_2}N_t^6\right) \log\left(\frac{1}{\vartheta}\right)\right)$, while I_{iter} represents the number of iterations.

V. NUMERICAL RESULTS AND DISCUSSION

In this section, numerical results are presented to prove the convergence and effectiveness of our algorithm. The positive direction of the X axis is used as the reference, and the azimuth angles of T_k ($K = 2$) and D relative to E are expressed as θ_{T_k} and θ_D , respectively. The direction of the radar detection range is $[-90^\circ, 90^\circ]$, σ^2 is normalized to be unity [14], [41], and other parameters are listed in Table IV.

Fig. 2(a) plots the beampattern gains of the JPT scheme with varying power budgets. It can be observed that the gains

of the mainlobe increases with increasing P_0 , while the width of the mainlobes remains unchanged. Fig. 2(b) demonstrates the relationship between DCRB and radar power budget for various schemes. It can be observed that the DCRB decreases with the increase of P_0 , which denotes that increasing the power budget can improve the accuracy of sensing. When $\rho = 0$, JPT is equivalent to the TSC scheme; when $\rho = 1$, JPT is equivalent to the PEC scheme. The JPT scheme's sensing performance outperforms that of the TSC scheme. This is because the beampattern gains in D 's direction is limited in the JPT scheme. With the increasing budget, more power is allocated to the mainlobe, enhancing the sensing performance. Fig. 2(c) plots the ER of various schemes versus the varying P_0 . We can find that both the PEC and JPT ($\rho \neq 0$) schemes obtain the maximum ER. The ER of the TSC and JPT with $\rho = 0$ are the worst exhibits no significant regular variation with the increase of P_0 . That is because (19e) and (19f) correspond to successful PE and the maximum interference at D , respectively and no maximizing ER in TSC and JPT with $\rho = 0$. Obviously, larger α_I , less ER due to α_I denotes the interference threshold at D .

Fig. 3(a) shows the relationship between the beampattern gains of the JPT scheme and N_t . The results show that the mainlobe's beampattern gains increases and its width decreases with increasing N_t . Fig. 3(b) demonstrates the sensing performance of all the schemes is improved with increasing N_t . Specifically, when the number of antennas is

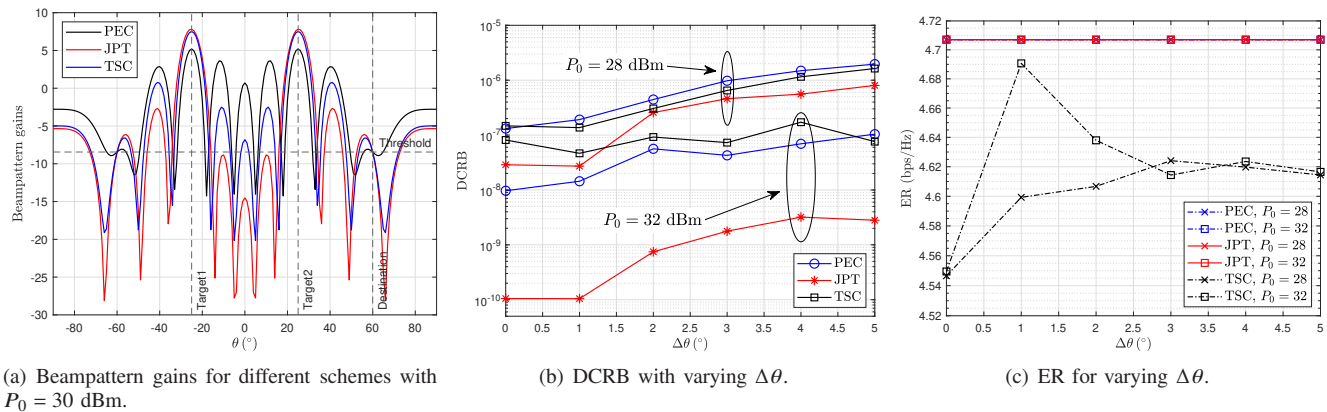


Fig. 4: The results versus varying P_0 with $\rho = 0.5$ and $N_t = 12$.

small, the TSC scheme's sensing performance is better than that of the JPT scheme. As the number of antennas increases, the JPT scheme's sensing performance increases faster than that of the TSC scheme. Moreover, the PEC scheme's sensing performance tends to be constant, which outperforms that of the TSC scheme since the beampattern gains in D 's direction is optimized so that more power is allocated to the mainlobe in the PEC scheme. Fig. 3(c) plots the ER for all the schemes versus varying N_t . We can find that both the PEC and JPT schemes reach the maximum ER at the beginning, and this rate remains constant regardless of the number of antennas. The TSC scheme's ER is the worst because only successful PE is guaranteed, and the minimum beampattern gains in the direction of D is given. Moreover, the increase of N_t enhances the beam gain, so the interference in the D 's direction increases, and the ER decreases. An interesting result is that, for the TSC scheme, the ER with a higher power budget ($P_0 = 30$ dBm) underperforms that with a lower power budget ($P_0 = 28$ dBm). This is because there is a constraint on the minimum gain in D 's direction in (17d), and as the power budget increases, the gains (interference power) in D 's direction also increases.

Fig. 4(a) plots the beampattern gains for the scenarios when target angles are perfectly known. It can be observed that the gain is maximum in the target direction and equal to the threshold in D 's direction. For the TSC scheme, the interference at D 's direction is slightly larger because the minimum gain in D 's direction is given in (17d). The essence of JPT design lies in the directional redistribution of beam energy by optimizing the gain of the target-direction beam while constraining energy allocation in specific directions (e.g., D -direction). This mechanism directly leads to its differentiated performance in non-target directions compared to TSC and PEC schemes, further validating the effectiveness of resource-coupled optimization in ISAC systems. Fig. 4(b) demonstrates the DCRB versus varying $\Delta\theta$ under different schemes. As the uncertain angle increases, the sensing performance of all the schemes deteriorates because the larger area needs to be covered with the given power. Moreover, the change of uncertain angle has a greater effect on the JPT's sensing performance than that of the TSC scheme. The sensing performance of the JPT scheme is better than that of the TSC at scenarios with

higher power, for the same reasons as Figs. 2(b) and 3(b). Fig. 4(c) shows the ER versus varying $\Delta\theta$ with different schemes. We can find that both the PEC and JPT schemes obtain the maximum ER, which is independent of the uncertain angle. For the TSC scheme, the ER increases with the increase of the uncertain angle because the range to be covered increases, and the interference in the D 's direction decreases. For a larger power ($P_0 = 32$ dBm), the interference in the D 's direction stays constant, thus the ER is independent of the uncertain angle.

Fig. 5(a) shows the beampattern gains of the JPT scheme with varying ρ . When $\rho = 1$, the mainlobe gain is minimum because the optimization objective in the JPT scheme reduces to minimizing the gains at D 's direction, which only maximizes the ER. Figs. 5(b)-5(d) plot the DCRB with varying ρ , respectively. One interesting conclusion can be observed that, in the JPT scheme, the DCRB remains constant for all ρ values except at the points where $\rho = 0$ and $\rho = 1$. The reason is that when $\rho = 0$, the JPT scheme degenerates to the TSC scheme; when $\rho = 1$, it degenerates to the PEC scheme. Comparing Figs. 5(b)-5(d), one can find that the sensing performance for all the schemes is improved as P_0 increases, which can also be found in Fig. 2(b). Furthermore, the JPT's sensing performance with ρ outperforms that of the TSC. This is because, in the JPT scheme, the beampattern gain in D 's direction is kept constant to maximize the ER. Then, more power is allocated to the mainlobe, resulting in better sensing performance.

Figs. 6(a)-6(c) plot the ER with varying ρ , respectively. It can be observed that, when $\rho \neq 0$, the ER of JPT is equal to that of PEC. Compared among Figs. 6(a)-6(c), the ER of all the schemes exhibits a relatively weak dependence on the P_0 , which can also be found in Fig. 2(c). It should be noted that the ER is equal to R_D , which is given in (8). Maximizing ER is equal to maximizing R_D , which is expressed as $\gamma_D = \frac{P_s |h_{SD}|^2}{\sigma_D^2}$ and is independent of P_0 . The ER of TSC shown in Figs. 6(a)-6(c) has a certain degree of randomness because the TSC scheme does not take into account maximizing ER, and ER is considered as a constraint (18f). It must be noted that the results in Figs. 5 and 6 clearly demonstrate that there is no trade-off between PE and TS. The core reason is as follows: the proposed joint optimization

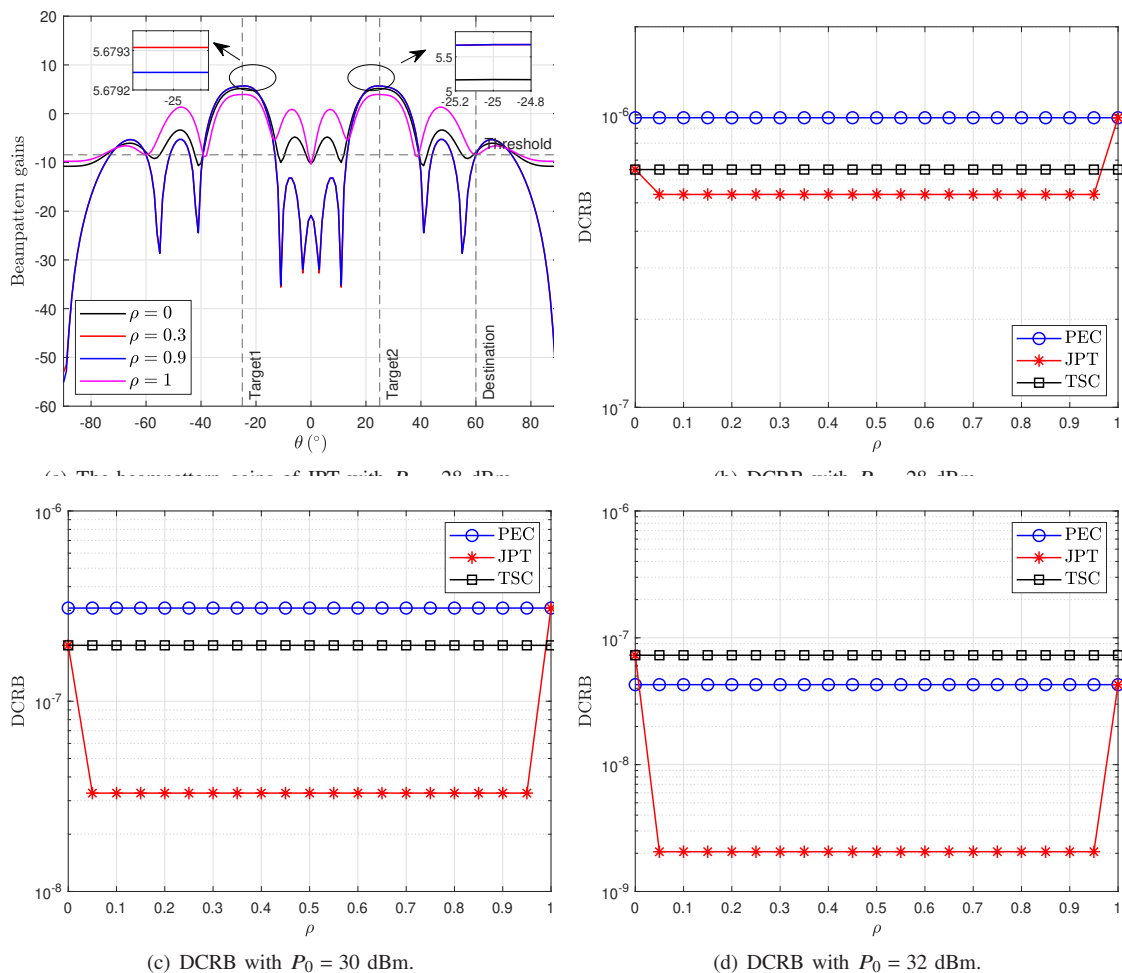


Fig. 5: The sensing performance with varying ρ .

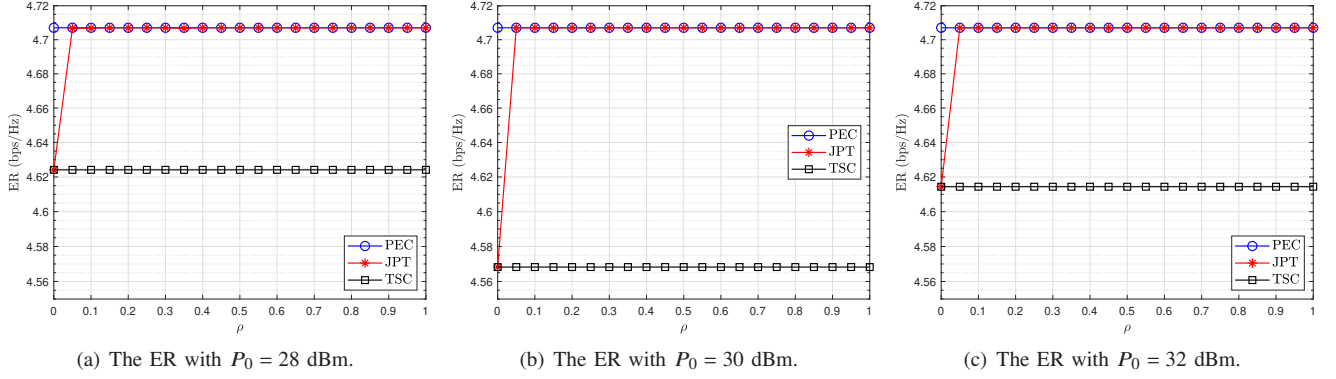
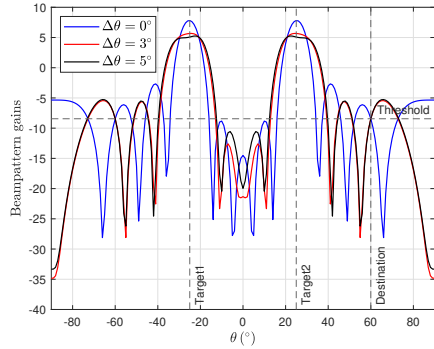
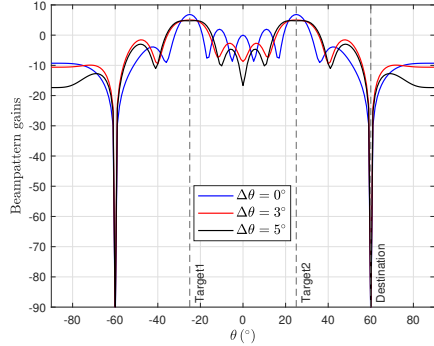
framework multiplexes radar waveforms to simultaneously transmit sensing signals and AN, which not only enables TS but also serves as AN to achieve successful PE. Specifically, by constraining the beam gain in the D 's direction, the ER can be maximized while ensuring successful PE. Meanwhile, the constrained energy in this direction enhances the degrees of freedom in energy distribution, thereby improving the TS performance. Consequently, the JPT design outperforms that of TSC and PEC.

Fig. 7(a) plots the beam pattern gains with uncertain angles for the JPT scheme. We can find that, with the increase of $\Delta\theta$, the mainlobe width becomes more expansive and the gain decreases because the energy is spread over a larger area. However, in the D 's direction, the gain must be not less than the requirement. Fig. 7(b) plots the beam pattern gains when the interference power is equal to zero. Because the quality of the eavesdropping channel is better than that of the illegal communication channel, it is not necessary to transmit power in D 's direction.

VI. CONCLUSION

This work studied the beamforming design in the joint PE and TS system wherein the multi-antenna BS transmits the signal to realize TS, which was utilized as AN to achieve

PE successfully. Firstly, two waveform design schemes were proposed to maximize the ER or minimize the DCRB only. Then, three waveform design schemes were investigated by formulating PE-centric, TS-centric, and normalized weighted optimization problems. By omitting the rank-one constraint, the non-convex problem was solved by the SDR technique. The SROCR method was utilized to solve continuously and iteratively to obtain the rank-one beamforming solution. In this work, it is assumed that the CSI and location of the illegal communication links are available. However, the channel estimation errors for illicit eavesdroppers also significantly affect practical results. The scenarios wherein the BS senses the illegal transmitters and receivers, and/or with the imperfect CSI of the unlawful links, will be part of future work.

Fig. 6: The PE performance with varying ρ .(a) Beampattern gains with non-zero interference ($d_{SE} = 1000$ m)(b) Beampattern gains with zero interference ($d_{SE} = 400$ m).Fig. 7: The beampattern gains versus varying $\Delta\theta$.

APPENDIX A DERIVATION OF CRB

The Fisher information matrix for $\zeta = [\theta, \beta_R, \beta_I]$ is expressed as

$$\begin{aligned} \mathbf{F} &= [\mathbf{F}(\zeta)_{ij}] \\ &= \left[\frac{2}{\sigma^2} \text{Re} \left[\frac{\partial (\mathbf{A}_r(\theta) \beta \mathbf{A}_t^H(\theta) \mathbf{x}_E)^H}{\partial \zeta_i} \frac{\partial (\mathbf{A}_r(\theta) \beta \mathbf{A}_t^H(\theta) \mathbf{x}_E)}{\partial \zeta_j} \right] \right] \\ &= \begin{bmatrix} \mathbf{F}(\theta, \theta) & \mathbf{F}(\theta, \beta_R) & \mathbf{F}(\theta, \beta_I) \\ \mathbf{F}(\beta_R, \theta) & \mathbf{F}(\beta_R, \beta_R) & \mathbf{F}(\beta_R, \beta_I) \\ \mathbf{F}(\beta_I, \theta) & \mathbf{F}(\beta_I, \beta_R) & \mathbf{F}(\beta_I, \beta_I) \end{bmatrix}, \end{aligned} \quad (25)$$

where $\mathbf{F}(\xi)_{ij} = \text{tr} \left[\mathbf{C}^{-1}(\xi) \frac{\partial \mathbf{C}(\xi)}{\partial \xi_i} \mathbf{C}^{-1}(\xi) \frac{\partial \mathbf{C}(\xi)}{\partial \xi_j} \right] + 2\text{Re} \left[\frac{\partial \mu^H(\xi)}{\partial \xi_i} \mathbf{C}^{-1}(\xi) \frac{\partial \mu(\xi)}{\partial \xi_j} \right]$ is a $K * K$ matrix.

1) The first element is expressed as

$$\mathbf{F}(\theta, \theta) = \begin{bmatrix} F(\theta_1, \theta_1) & \dots & F(\theta_1, \theta_K) \\ \dots & F(\theta_i, \theta_j) & \dots \\ F(\theta_K, \theta_1) & \dots & F(\theta_K, \theta_K) \end{bmatrix}, \quad (26)$$

where $F(\theta_i, \theta_j)$ is obtained as (27), shown at the top of the next page, where $F_{11} = (\mathbf{A}_r^H \dot{\mathbf{A}}_r) \odot (\beta^* \dot{\mathbf{A}}_t^H \mathbf{R}^* \mathbf{A}_t \beta) + (\mathbf{A}_r^H \dot{\mathbf{A}}_r) \odot (\beta^* \dot{\mathbf{A}}_t^H \mathbf{R}^* \dot{\mathbf{A}}_t \beta) + (\dot{\mathbf{A}}_r^H \dot{\mathbf{A}}_r) \odot (\beta^* \mathbf{A}_t^H \mathbf{R}^* \mathbf{A}_t \beta) + (\dot{\mathbf{A}}_r^H \dot{\mathbf{A}}_r) \odot (\beta^* \mathbf{A}_t^H \mathbf{R}^* \dot{\mathbf{A}}_t \beta)$, $[\mathbf{B}]_{ij}$ denotes the (i, j) element of the matrix \mathbf{B} , e_i denotes the i -th column of the identity matrix, step (a) holds by

$$\frac{\partial (\mathbf{A}_r \beta \mathbf{A}_t^T \mathbf{x}_E)}{\partial \theta_i} = \dot{\mathbf{A}}_r e_i e_i^T \beta \mathbf{A}_t^T \mathbf{x}_E + \mathbf{A}_r \beta \dot{\mathbf{A}}_t^T e_i e_i^T \mathbf{x}_E, \quad (28)$$

step (b) holds by

$$\begin{aligned} &\text{tr} \left[(\mathbf{x}_E^H e_i e_i^T \dot{\mathbf{A}}_t^* \beta^H \mathbf{A}_r^H) (\dot{\mathbf{A}}_r e_j e_j^T \beta \mathbf{A}_t^T \mathbf{x}_E) \right] \\ &= e_i^T (\mathbf{A}_r^H \dot{\mathbf{A}}_r) e_j e_j^T (\beta \mathbf{A}_t^T \mathbf{x}_E \mathbf{x}_E^H \dot{\mathbf{A}}_t^* \beta^H) e_i \\ &= L(\mathbf{A}_r^H \dot{\mathbf{A}}_r)_{ij} (\beta^* \mathbf{A}_t^H \mathbf{R}^* \mathbf{A}_t \beta)_{ij}, \end{aligned} \quad (29)$$

and step (c) holds by

$$L(\mathbf{A}_r^H \dot{\mathbf{A}}_r)_{ij} (\beta^* \mathbf{A}_t^H \mathbf{R}^* \mathbf{A}_t \beta)_{ij} = [\mathbf{A}_r^H \dot{\mathbf{A}}_r \odot \beta^* \mathbf{A}_t^H \mathbf{R}^* \mathbf{A}_t \beta]_{ij}. \quad (30)$$

2) The element of $\mathbf{F}(\theta, \beta_R)$ is expressed as

$$\begin{aligned} F(\theta_i, b_{R_j}) &= \frac{2}{\sigma^2} \text{Re} \left[\frac{\partial (\mathbf{A}_r \beta \mathbf{A}_t^T \mathbf{x}_E)^H}{\partial \theta_i} \frac{\partial (\mathbf{A}_r \beta \mathbf{A}_t^T \mathbf{x}_E)}{\partial b_{R_j}} \right] \\ &= \frac{2}{\sigma^2} \text{Re} \left[L(\mathbf{A}_r^H \dot{\mathbf{A}}_r)_{ij} (\beta^* \mathbf{A}_t^H \mathbf{R}^* \mathbf{A}_t)_{ij} \right. \\ &\quad \left. + L(\dot{\mathbf{A}}_r^H \mathbf{A}_r)_{ij} (\beta^* \mathbf{A}_t^H \mathbf{R}^* \mathbf{A}_t)_{ij} \right] \\ &= \frac{2}{\sigma^2} [\text{Re}(\mathbf{F}_{12})]_{ij} \end{aligned} \quad (31)$$

where $F_{12} = (\mathbf{A}_r^H \dot{\mathbf{A}}_r) \odot (\beta^* \dot{\mathbf{A}}_t^H \mathbf{R}^* \mathbf{A}_t) + (\dot{\mathbf{A}}_r^H \mathbf{A}_r) \odot (\beta^* \mathbf{A}_t^H \mathbf{R}^* \mathbf{A}_t)$ and $\frac{\partial (\mathbf{A}_r \beta \mathbf{A}_t^T \mathbf{x}_E)}{\partial b_{R_j}} = \mathbf{A}_r e_j e_j^T \mathbf{A}_t^T \mathbf{x}_E$.

$$\begin{aligned}
F(\theta_i, \theta_j) &= \frac{2}{\sigma^2} \text{Retr} \left[\frac{\partial (\mathbf{A}_r \beta \mathbf{A}_t^T \mathbf{x}_E)^H}{\partial \theta_i} \frac{\partial (\mathbf{A}_r \beta \mathbf{A}_t^T \mathbf{x}_E)}{\partial \theta_j} \right] \\
&\stackrel{(a)}{=} \frac{2}{\sigma^2} \text{Retr} \left[\left(\mathbf{x}_E^H e_i e_i^T \dot{\mathbf{A}}_t^* \beta^H \mathbf{A}_r^H + \mathbf{x}_E^H \mathbf{A}_t^* \beta^H e_i e_i^T \dot{\mathbf{A}}_r^H \right) \times \left(\dot{\mathbf{A}}_r e_j e_j^T \beta \mathbf{A}_t^T \mathbf{x}_E + \mathbf{A}_r \beta \dot{\mathbf{A}}_t^T e_j e_j^T \mathbf{x}_E \right) \right] \\
&= \frac{2}{\sigma^2} \text{Retr} \left[\mathbf{x}_E^H e_i e_i^T \mathbf{A}_t^* \beta^H \mathbf{A}_r^H \mathbf{A}_r e_j e_j^T \beta \mathbf{A}_t^T \mathbf{x}_E + \mathbf{x}_E^H e_i e_i^T \mathbf{A}_t^* \beta^H \mathbf{A}_r^H \mathbf{A}_r \beta \mathbf{A}_t^T e_j e_j^T \mathbf{x}_E \right. \\
&\quad \left. + \mathbf{x}_E^H \mathbf{A}_t^* \beta^H e_i e_i^T \dot{\mathbf{A}}_r^H \mathbf{A}_r e_j e_j^T \beta \mathbf{A}_t^T \mathbf{x}_E + \mathbf{x}_E^H \mathbf{A}_t^* \beta^H e_i e_i^T \dot{\mathbf{A}}_r^H \mathbf{A}_r \beta \mathbf{A}_t^T e_j e_j^T \mathbf{x}_E \right] \\
&\stackrel{(b)}{=} \frac{2}{\sigma^2} \text{Re} \left[e_i^T \left(\mathbf{A}_r^H \mathbf{A}_r \right) e_j e_j^T \left(\beta \mathbf{A}_t^T \mathbf{x}_E \mathbf{x}_E^H \mathbf{A}_t^* \beta^H \right) e_i + e_i^T \left(\mathbf{A}_r^H \mathbf{A}_r \right) e_j e_j^T \left(\beta \mathbf{A}_t^T \mathbf{x}_E \mathbf{x}_E^H \mathbf{A}_t^* \beta^H \right) e_i \right. \\
&\quad \left. + e_i^T \left(\mathbf{A}_r^H \mathbf{A}_r \right) e_j e_j^T \left(\beta \mathbf{A}_t^T \mathbf{x}_E \mathbf{x}_E^H \mathbf{A}_t^* \beta^H \right) e_i + e_i^T \left(\mathbf{A}_r^H \mathbf{A}_r \right) e_j e_j^T \left(\beta \mathbf{A}_t^T \mathbf{x}_E \mathbf{x}_E^H \mathbf{A}_t^* \beta^H \right) e_i \right] \\
&\stackrel{(c)}{=} \frac{2}{\sigma^2} \text{Re} \left[L \left(\mathbf{A}_r^H \mathbf{A}_r \right)_{ij} \left(\beta^* \mathbf{A}_t^H \mathbf{R}^* \mathbf{A}_t \beta \right)_{ij} + L \left(\mathbf{A}_r^H \mathbf{A}_r \right)_{ij} \left(\beta^* \mathbf{A}_t^H \mathbf{R}^* \mathbf{A}_t \beta \right)_{ij} \right. \\
&\quad \left. + L \left(\mathbf{A}_r^H \mathbf{A}_r \right)_{ij} \left(\beta^* \mathbf{A}_t^H \mathbf{R}^* \mathbf{A}_t \beta \right)_{ij} + L \left(\mathbf{A}_r^H \mathbf{A}_r \right)_{ij} \left(\beta^* \mathbf{A}_t^H \mathbf{R}^* \mathbf{A}_t \beta \right)_{ij} \right] \\
&= \frac{2}{\sigma^2} [\text{Re}(\mathbf{F}_{11})]_{ij} \tag{27}
\end{aligned}$$

3) The element of $\mathbf{F}(\theta, \beta_I)$, $\mathbf{F}(\beta_R, \theta)$, $\mathbf{F}(\beta_R, \beta_R)$, $\mathbf{F}(\beta_R, \beta_I)$, $\mathbf{F}(\beta_I, \theta)$, $\mathbf{F}(\beta_I, \beta_R)$, and $\mathbf{F}(\beta_I, \beta_I)$ are expressed as

$$\begin{aligned}
F(\theta_i, b_{I_j}) &= \frac{2}{\sigma^2} \text{Retr} \left[\frac{\partial (\mathbf{A}_r \beta \mathbf{A}_t^T \mathbf{x}_E)^H}{\partial \theta_i} \frac{\partial (\mathbf{A}_r \beta \mathbf{A}_t^T \mathbf{x}_E)}{\partial b_{I_j}} \right] \\
&= \frac{2}{\sigma^2} \text{Re} \left[L \left(j \mathbf{A}_r^H \dot{\mathbf{A}}_r \right)_{ij} \left(\beta^* \dot{\mathbf{A}}_t^H \mathbf{R}^* \mathbf{A}_t \right)_{ij} \right. \\
&\quad \left. + L \left(j \dot{\mathbf{A}}_r^H \mathbf{A}_r \right)_{ij} \left(\beta^* \mathbf{A}_t^H \mathbf{R}^* \mathbf{A}_t \right)_{ij} \right] \\
&= -\frac{2}{\sigma^2} [\text{Im}(\mathbf{F}_{12})]_{ij}, \tag{32}
\end{aligned}$$

$$\begin{aligned}
F(b_{R_i}, \theta_j) &= \frac{2}{\sigma^2} \text{Re} \left[L \left(\mathbf{A}_r^H \mathbf{A}_r \right)_{ij} \left(\mathbf{A}_t^H \mathbf{R}^* \dot{\mathbf{A}}_t \beta \right)_{ij} \right. \\
&\quad \left. + L \left(\mathbf{A}_r^H \dot{\mathbf{A}}_r \right)_{ij} \left(\mathbf{A}_t^H \mathbf{R}^* \mathbf{A}_t \beta \right)_{ij} \right] \\
&= \frac{2}{\sigma^2} [\text{Re}^T(\mathbf{F}_{12})]_{ij}, \tag{33}
\end{aligned}$$

$$\begin{aligned}
F(b_{R_i}, b_{R_j}) &= \frac{2}{\sigma^2} \text{Retr} \left[\left(\mathbf{x}_E^H \mathbf{A}_t^* e_i e_i^T \mathbf{A}_r^H \right) \left(\mathbf{A}_r e_j e_j^T \mathbf{A}_t^T \mathbf{x}_E \right) \right] \\
&= \frac{2}{\sigma^2} \text{Re} \left[L \left(\mathbf{A}_r^H \mathbf{A}_r \right)_{ij} \left(\mathbf{A}_t^H \mathbf{R}^* \mathbf{A}_t \right)_{ij} \right] \\
&= \frac{2}{\sigma^2} [\text{Re}(\mathbf{F}_{22})]_{ij}, \tag{34}
\end{aligned}$$

$$\begin{aligned}
F(b_{R_i}, b_{I_j}) &= \frac{2}{\sigma^2} \text{Retr} \left[\left(\mathbf{x}_E^H e_i e_i^T \mathbf{A}_t^* \mathbf{A}_r^H \right) \left(j \mathbf{A}_r e_j e_j^T \mathbf{A}_t^T \mathbf{x}_E \right) \right] \\
&= \frac{2}{\sigma^2} \text{Re} \left[L \left(j \mathbf{A}_r^H \mathbf{A}_r \right)_{ij} \left(\mathbf{A}_t^H \mathbf{R}^* \mathbf{A}_t \right)_{ij} \right] \\
&= -\frac{2}{\sigma^2} [\text{Im}^T(\mathbf{F}_{22})]_{ij}, \tag{35}
\end{aligned}$$

$$\begin{aligned}
F(b_{I_i}, \theta_j) &= \frac{2}{\sigma^2} \text{Re} \left[L \left(-j \mathbf{A}_r^H \dot{\mathbf{A}}_r \right)_{ij} \left(\mathbf{A}_t^H \mathbf{R}^* \mathbf{A}_t \beta \right)_{ij} \right. \\
&\quad \left. + L \left(-j \dot{\mathbf{A}}_r^H \mathbf{A}_r \right)_{ij} \left(\mathbf{A}_t^H \mathbf{R}^* \mathbf{A}_t \beta \right)_{ij} \right] \\
&= -\frac{2}{\sigma^2} [\text{Im}^T(\mathbf{F}_{12})]_{ij}, \tag{36}
\end{aligned}$$

$$\begin{aligned}
F(b_{I_i}, b_{R_j}) &= \frac{2}{\sigma^2} \text{Retr} \left[\left(-j \mathbf{x}_E^H \mathbf{A}_t^* e_i e_i^T \mathbf{A}_r^H \right) \left(\mathbf{A}_r e_j e_j^T \mathbf{A}_t^T \mathbf{x}_E \right) \right] \\
&= \frac{2}{\sigma^2} \text{Re} \left[L \left(-j \mathbf{A}_r^H \mathbf{A}_r \right)_{ij} \left(\mathbf{A}_t^H \mathbf{R}^* \mathbf{A}_t \right)_{ij} \right] \\
&= -\frac{2}{\sigma^2} [\text{Im}^T(\mathbf{F}_{22})]_{ij}, \tag{37}
\end{aligned}$$

$$\begin{aligned}
F(b_{I_i}, b_{I_j}) &= \frac{2}{\sigma^2} \text{Retr} \left[\left(-j \mathbf{x}_E^H \mathbf{A}_t^* e_i e_i^T \mathbf{A}_r^H \right) \left(j \mathbf{A}_r e_j e_j^T \mathbf{A}_t^T \mathbf{x}_E \right) \right] \\
&= \frac{2}{\sigma^2} \text{Re} \left[L \left(\mathbf{A}_r^H \mathbf{A}_r \right)_{ij} \left(\mathbf{A}_t^H \mathbf{R}^* \mathbf{A}_t \right)_{ij} \right] \\
&= \frac{2}{\sigma^2} [\text{Re}^T(\mathbf{F}_{22})]_{ij}, \tag{38}
\end{aligned}$$

where $F_{22} = (\mathbf{A}_r^H \mathbf{A}_r) \odot (\mathbf{A}_t^H \mathbf{R}^* \mathbf{A}_t)$ and $\frac{\partial (\mathbf{A}_r \beta \mathbf{A}_t^T \mathbf{x}_E)}{\partial b_{I_j}} = j \mathbf{A}_r e_j e_j^T \mathbf{A}_t^T \mathbf{x}_E$.

REFERENCES

- [1] F. Liu, Y. Cui, C. Masouros, J. Xu, T. X. Han, Y. C. Eldar, and S. Buzzi, "Integrated sensing and communications: Towards dual-functional wireless networks for 6G and beyond," *IEEE J. Sel. Areas Commun.*, vol. 40, no. 6, pp. 1728-1767, Jun. 2022.
- [2] F. Dong, F. Liu, Y. Cui, W. Wang, K. Han, and Z. Wang, "Sensing as a service in 6G perceptive networks: A unified framework for ISAC resource allocation," *IEEE Trans. Wireless Commun.*, vol. 22, no. 5, pp. 3522-3536, May 2023.
- [3] Z. Wei, H. Qu, Y. Wang, X. Yuan, H. Wu, Y. Du, K. Han, N. Zhang, and Z. Feng, "Integrated sensing and communication signals toward 5G-A and 6G: A survey," *IEEE Internet Things J.*, vol. 10, no. 13, pp. 11068-11092, Jul. 2023.

- [4] Z. Wei, F. Liu, C. Masouros, N. Su, and A. P. Petropulu, "Toward multi-functional 6G wireless networks: Integrating sensing, communication, and security," *IEEE Commun. Mag.*, vol. 60, no. 4, pp. 65-71, Apr. 2022.
- [5] W. Ni, W. Wang, A. Zheng, P. Wang, C. You, Y. C. Eldar, D. Niyato, and R. Schober, "Two birds with one stone: Enhancing communication and sensing via multi-functional RIS," *IEEE Wireless Commun.*, vol. 32, no. 4, pp. 72-80, Aug. 2025.
- [6] F. Liu, Y.-F. Liu, A. Li, C. Masouros, and Y. C. Eldar, "Cramér-Rao bound optimization for joint radar-communication beamforming," *IEEE Trans. Signal Process.*, vol. 70, pp. 240-253, Dec. 2022.
- [7] C. Wen, Y. Huang, L. Zheng, W. J. Liu, and T. N. Davidson, "Transmit waveform design for dual-function radar-communication systems via hybrid linear-nonlinear precoding," *IEEE Trans. Signal Process.*, vol. 71, pp. 2130-2145, Jun. 2023.
- [8] Z. Ren, Y. Peng, X. Song, Y. Fang, L. Qiu, L. Liu, D. W. K. Ng, and J. Xu, "Fundamental CRB-rate tradeoff in multi-antenna ISAC systems with information multicasting and multi-target sensing," *IEEE Trans. Wireless Commun.*, vol. 23, no. 4, pp. 3870-3885, Apr. 2024.
- [9] Z. Zhao, L. Zhang, R. Jiang, X.-P. Zhang, X. Tang, and Y. Dong, "Joint beamforming scheme for ISAC systems via robust Cramér-Rao bound optimization," *IEEE Wireless Commun. Lett.*, vol. 13, no. 3, pp. 889-893, Mar. 2024.
- [10] X. Li, F. Liu, Z. Zhou, G. Zhu, S. Wang, K. Huang, and Y. Gong, "Integrated sensing, communication, and computation over-the-air: MIMO beamforming design," *IEEE Trans. Wireless Commun.*, vol. 22, no. 8, pp. 5383-5398, Aug. 2023.
- [11] T. Liu, Y. Guo, L. Lu, and B. Xia, "Waveform design for integrated sensing and communication systems based on interference exploitation," *J. Commun. Inform. Netw.*, vol. 7, no. 4, pp. 447-456, Dec. 2022.
- [12] R. Liu, M. Li, Q. Liu, and A. L. Swindlehurst, "SNR/CRB-constrained joint beamforming and reflection designs for RIS-ISAC systems," *IEEE Trans. Wireless Commun.*, vol. 23, no. 7, pp. 7456-7470, Jul. 2024.
- [13] F. Xia, Z. Fei, X. Wang, W. Yuan, Q. Wu, Y. Liu, and T. Q. S. Quek, "Symbiotic sensing and communication: Framework and beamforming design," *IEEE Trans. Wireless Commun.*, vol. 24, no. 3, pp. 2417-2434, Mar. 2025.
- [14] H. Hua, T. X. Han, and J. Xu, "MIMO integrated sensing and communication: CRB-rate tradeoff," *IEEE Trans. Wireless Commun.*, vol. 23, no. 4, pp. 2839-2854, Apr. 2024.
- [15] G. Wu, Y. Fang, J. Xu, Z. Feng, and S. Cui, "Energy-efficient MIMO integrated sensing and communications with on-off non-transmission powers," *IEEE Internet Things J.*, vol. 11, no. 7, pp. 12177-12191, Apr. 2024.
- [16] Z. He, W. Xu, H. Shen, D. W. K. Ng, Y. C. Eldar, and X. You, "Full-duplex communication for ISAC: Joint beamforming and power optimization," *IEEE J. Sel. Areas Commun.*, vol. 41, no. 9, pp. 2920-2936, Sep. 2023.
- [17] Y. Guo, Y. Liu, Q. Wu, X. Li, and Q. Shi, "Joint beamforming and power allocation for RIS aided full-duplex integrated sensing and uplink communication system," *IEEE Trans. Wireless Commun.*, vol. 23, no. 5, pp. 4627-4642, May 2024.
- [18] Y. Dong, F. Liu, and Y. Xiong, "Joint receiver design for integrated sensing and communications," *IEEE Commun. Lett.*, vol. 27, no. 7, pp. 1854-1858, Jul. 2023.
- [19] C. Ouyang, Y. Liu, and H. Yang, "Revealing the impact SIC in NOMA-ISAC," *IEEE Wireless Commun. Lett.*, vol. 12, no. 10, pp. 1707-1711, Oct. 2023.
- [20] N. Su, F. Liu, and C. Masouros, "Secure radar-communication systems with malicious targets: Integrating radar, communications and jamming functionalities," *IEEE Trans. Wireless Commun.*, vol. 20, no. 1, pp. 83-95, Jan. 2021.
- [21] N. Su, F. Liu, Z. Wei, Y.-F. Liu, and C. Masouros, "Secure dual-functional radar-communication transmission: Exploiting interference for resilience against target eavesdropping," *IEEE Trans. Wireless Commun.*, vol. 21, no. 9, pp. 7238-7252, Sept. 2022.
- [22] H. Jia, X. Li, and L. Ma, "Physical layer security optimization with Cramér-Rao bound metric in ISAC systems under sensing-specific imperfect CSI model," *IEEE Trans. Veh. Technol.*, vol. 73, no. 5, pp. 6980-6992, May 2024.
- [23] W. Wei, X. Pang, C. Xing, N. Zhao, and D. Niyato, "STAR-RIS aided secure NOMA integrated sensing and communication," *IEEE Trans. Wireless Commun.*, vol. 23, no. 9, pp. 10712-10725, Sept. 2024.
- [24] F. Dong, W. Wang, X. Li, F. Liu, S. Chen, and L. Hanzo, "Joint beamforming design for dual-functional MIMO radar and communication systems guaranteeing physical layer security," *IEEE Trans. Green Commun. Netw.*, vol. 7, no. 1, pp. 537-549, Mar. 2023.
- [25] Z. Ren, L. Qiu, J. Xu, and D. W. K. Ng, "Robust transmit beamforming for secure integrated sensing and communication," *IEEE Trans. Commun.*, vol. 71, no. 9, pp. 5549-5564, Sep. 2023.
- [26] N. Su, F. Liu, and C. Masouros, "Sensing-assisted eavesdropper estimation: An ISAC breakthrough in physical layer security," *IEEE Trans. Wireless Commun.*, vol. 23, no. 4, pp. 3162-3174, Apr. 2024.
- [27] J. Chu, R. Liu, M. Li, Y. Liu, and Q. Liu, "Joint secure transmit beamforming designs for integrated sensing and communication systems," *IEEE Trans. Veh. Technol.*, vol. 72, no. 4, pp. 4778-4791, Apr. 2023.
- [28] J. Zhang, J. Xu, W. Lu, N. Zhao, X. Wang, and D. Niyato, "Secure transmission for IRS-aided UAV-ISAC networks," *IEEE Trans. Wireless Commun.*, vol. 23, no. 9, pp. 12256-12269, Sep. 2024.
- [29] Q. Dan, H. Lei, K.-H. Park, and G. Pan, "Beamforming for secure RSMA-aided ISAC systems," *IEEE Trans. Cogn. Commun. Netw.*, doi: 10.1109/TCCN.2025.3587100, Jun. 2025.
- [30] Q. Dan, H. Lei, K.-H. Park, W. Lei, and G. Pan, "Proactive eavesdropping in relay systems via trajectory and power optimization," *IEEE Internet Things J.*, vol. 11, no. 21, Oct. 2024.
- [31] Y. Zeng and R. Zhang, "Wireless information surveillance via proactive eavesdropping with spoofing relay," *IEEE J. Sel. Topics Signal Process.*, vol. 10, no. 8, pp. 1449-1461, Dec. 2016.
- [32] D. Guo, H. Ding, L. Tang, X. Zhang, and Y.-C. Liang, "Wireless surveillance in a MIMO system with spoofing relay and UAV-enabled eavesdropper," *IEEE Trans. Veh. Technol.*, vol. 73, no. 10, pp. 15792-15797, Oct. 2024.
- [33] J. Xu, L. Duan, and R. Zhang, "Proactive eavesdropping via cognitive jamming in fading channels," *IEEE Trans. Wireless Commun.*, vol. 16, no. 5, pp. 2790-2806, May 2017.
- [34] S. Hu, Q. Wu, and X. Wang, "Energy management and trajectory optimization for UAV-enabled legitimate monitoring systems," *IEEE Trans. Wireless Commun.*, vol. 20, no. 1, pp. 142-155, Jan. 2021.
- [35] D. Xu and H. Zhu, "Jamming-assisted legitimate eavesdropping and secure communication in multicarrier interference networks," *IEEE Syst. J.*, vol. 16, no. 1, pp. 954-965, Mar. 2022.
- [36] F. Feizi, M. Mohammadi, Z. Mobini, and C. Tellambura, "Proactive eavesdropping via jamming in full-duplex multi-antenna systems: Beamforming design and antenna selection," *IEEE Trans. Commun.*, vol. 68, no. 12, pp. 7563-7577, Dec. 2020.
- [37] H. Zhang, L. Duan, and R. Zhang, "Jamming-assisted proactive eavesdropping over two suspicious communication links," *IEEE Trans. Wireless Commun.*, vol. 19, no. 7, pp. 4817-4830, Jul. 2020.
- [38] B. Li, Y. Yao, H. Zhang, and Y. Lv, "Energy efficiency of proactive cooperative eavesdropping over multiple suspicious communication links," *IEEE Trans. Veh. Technol.*, vol. 68, no. 1, pp. 420-430, Jan. 2019.
- [39] J. Moon, H. Lee, C. Song, S. Lee, and I. Lee, "Proactive eavesdropping with full-duplex relay and cooperative jamming," *IEEE Trans. Wireless Commun.*, vol. 17, no. 10, pp. 6707-6719, Oct. 2018.
- [40] H. Lei, R. Gao, K.-H. Park, I. S. Ansari, K. J. Kim, and M.-S. Alouini, "On secure downlink NOMA systems with outage constraint," *IEEE Trans. Commun.*, vol. 68, no. 12, pp. 7824-7836, Dec. 2020.
- [41] J. Li, L. Xu, P. Stoica, K. W. Forsythe, and D. W. Bliss, "Range compression and waveform optimization for MIMO radar: A Cramér-Rao bound based study," *IEEE Trans. Signal Process.*, vol. 56, no. 1, pp. 218-232, Jan. 2008.
- [42] M. Hua, L. Yang, Q. Wu, and A. L. Swindlehurst, "3D UAV trajectory and communication design for simultaneous uplink and downlink transmission," *IEEE Trans. Commun.*, vol. 68, no. 9, pp. 5908-5923, Sept. 2020.
- [43] H. Lei, J. Jiang, H. Yang, K.-H. Park, I. S. Ansari, G. Pan, and M.-S. Alouini, "Trajectory and power design for aerial CRNs with colluding eavesdroppers," *IEEE Trans. Veh. Technol.*, vol. 73, no. 12, Aug. 2024.
- [44] X. Jiang, H. Lin, C. Zhong, X. Chen, and Z. Zhang, "Proactive eavesdropping in relaying systems," *IEEE Signal Process. Lett.*, vol. 24, no. 6, pp. 917-921, Jun. 2017.
- [45] R. He, G. Li, J. Chen, H. Wang, X. Guan, Y. Xu, W. He, and Y. Xu, "Joint power and beamformer optimization in multi-antenna relay covert system: Exploiting public users as shelter," *IEEE Trans. Wireless Commun.*, vol. 24, no. 1, pp. 385-400, Jan. 2025.
- [46] P. Cao, J. Thompson, and H. V. Poor, "A sequential constraint relaxation algorithm for rank-one constrained problems," in *Proc. 25th European Signal Processing Conference (EUSIPCO)*, Kos, Greece, Aug. 2017, pp. 1060-1064.
- [47] Z. Liu, X. Li, H. Ji, H. Zhang, and V. C. M. Leung, "Toward STAR-RIS-empowered integrated sensing and communications: Joint active and passive beamforming design," *IEEE Trans. Veh. Technol.*, vol. 72, no. 12, pp. 15991-16005, Dec. 2023.